

NAVAL POSTGRADUATE SCHOOL Monterey, California



THESIS

**SEAWIFS ANALYSIS OF THE JAPAN AND EAST CHINA
SEA AIR/SEA ENVIRONMENT**

by

James D. Rocha

December 2001

Thesis Advisor:

Philip A. Durkee

Co-Advisor:

Steven R. Ramp

Approved for public release; distribution is unlimited.

Report Documentation Page

Report Date 19 Dec 2001	Report Type N/A	Dates Covered (from... to) -
Title and Subtitle SEAWIFS Ananlysis of the Japan and East China Sea Air/Sea Environment	Contract Number	
	Grant Number	
	Program Element Number	
Author(s) Rocha, James	Project Number	
	Task Number	
	Work Unit Number	
Performing Organization Name(s) and Address(es) Naval Postgraduate School Monterey, California	Performing Organization Report Number	
Sponsoring/Monitoring Agency Name(s) and Address(es)	Sponsor/Monitor's Acronym(s)	
	Sponsor/Monitor's Report Number(s)	
Distribution/Availability Statement Approved for public release, distribution unlimited		
Supplementary Notes The original document contains color images.		
Abstract		
Subject Terms		
Report Classification unclassified	Classification of this page unclassified	
Classification of Abstract unclassified	Limitation of Abstract UU	
Number of Pages 81		

THIS PAGE INTENTIONALLY LEFT BLANK

REPORT DOCUMENTATION PAGE			<i>Form Approved OMB No. 0704-0188</i>	
Public reporting burden for this collection of information is estimated to average 1 hour per response, including the time for reviewing instruction, searching existing data sources, gathering and maintaining the data needed, and completing and reviewing the collection of information. Send comments regarding this burden estimate or any other aspect of this collection of information, including suggestions for reducing this burden, to Washington headquarters Services, Directorate for Information Operations and Reports, 1215 Jefferson Davis Highway, Suite 1204, Arlington, VA 22202-4302, and to the Office of Management and Budget, Paperwork Reduction Project (0704-0188) Washington DC 20503.				
1. AGENCY USE ONLY (Leave blank)		2. REPORT DATE December 2001	3. REPORT TYPE AND DATES COVERED Master's Thesis	
4. TITLE AND SUBTITLE: SeaWiFS analysis of the Japan and East China Sea air/sea environment			5. FUNDING NUMBERS	
6. AUTHOR(S) James D. Rocha				
7. PERFORMING ORGANIZATION NAME(S) AND ADDRESS(ES) Naval Postgraduate School Monterey, CA 93943-5000			8. PERFORMING ORGANIZATION REPORT NUMBER	
9. SPONSORING / MONITORING AGENCY NAME(S) AND ADDRESS(ES) N/A			10. SPONSORING / MONITORING AGENCY REPORT NUMBER	
11. SUPPLEMENTARY NOTES The views expressed in this thesis are those of the author and do not reflect the official policy or position of the Department of Defense or the U.S. Government.				
12a. DISTRIBUTION / AVAILABILITY STATEMENT Approved for public release; distribution is unlimited			12b. DISTRIBUTION CODE	
13. ABSTRACT (maximum 200 words) Using visible wavelength radiance data obtained from the spaceborne Sea-viewing Wide Field-of-view Sensor (SeaWiFS), during the Aerosol Characterization Experiment-Asia (ACE-Asia), an analysis of the Japan and East China Sea regions was completed to determine the background ocean reflectance characteristics and distribution, the effects of both ocean turbidity and various aerosols on the radiance received from the top of the atmosphere, and develop algorithms designed to identify areas of airborne dust and high ocean turbidity. The primary objective of the analysis was to better characterize and parameterize the regional background reflectance in order to improve the accuracy of the aerosol optical depth algorithms currently in use. A secondary objective was to develop a method of determining the geographic extent and basic intensity of the ocean turbidity. The intent of the study was to explore how visible wavelength solar radiation is affected by its interaction with the regional environment. The work has operational significance because many types of military systems operate using visible wavelength energy and are greatly affected by scattering particles either airborne or suspended in the water column. The types of systems affected range from imaging and targeting to mine hunting and identification equipment.				
14. SUBJECT TERMS Sea-viewing Wide Field-of-view Sensor, SeaWiFS, Japan Sea, East China Sea, aerosol optical depth, turbidity, dust.			15. NUMBER OF PAGES 81	
			16. PRICE CODE	
17. SECURITY CLASSIFICATION OF REPORT Unclassified	18. SECURITY CLASSIFICATION OF THIS PAGE Unclassified	19. SECURITY CLASSIFICATION OF ABSTRACT Unclassified	20. LIMITATION OF ABSTRACT UL	

THIS PAGE INTENTIONALLY LEFT BLANK

Approved for public release; distribution unlimited.

SEAWIFS ANALYSIS OF THE JAPAN AND EAST CHINA SEA AIR/SEA ENVIRONMENT

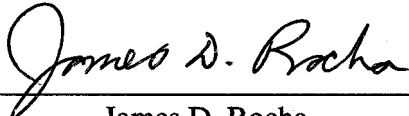
James D. Rocha
Lieutenant Commander, United States Navy
B.S., Regents College, 1996

Submitted in partial fulfillment of the
requirements for the degree of

MASTER OF SCIENCE IN PHYSICAL OCEANOGRAPHY

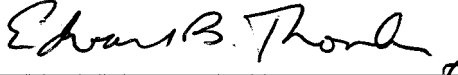
from the

**NAVAL POSTGRADUATE SCHOOL
December 2001**

Author: 
James D. Rocha

Approved by: 
Philip A. Durkee, Thesis Advisor


Steven R. Ramp, Co-Advisor


Mary L. Batteen, Chairperson
Department of Oceanography

THIS PAGE INTENTIONALLY LEFT BLANK

ABSTRACT

Using visible wavelength radiance data obtained from the spaceborne Sea-viewing Wide Field-of-view Sensor (SeaWiFS), during the Aerosol Characterization Experiment-Asia (ACE-Asia), an analysis of the Japan and East China Sea regions was completed to determine the background ocean reflectance characteristics and distribution, the effects of both ocean turbidity and various aerosols on the radiance received from the top of the atmosphere, and develop algorithms designed to identify areas of airborne dust and high ocean turbidity. The primary objective of the analysis was to better characterize and parameterize the regional background reflectance in order to improve the accuracy of the aerosol optical depth algorithms currently in use. A secondary objective was to develop a method of determining the geographic extent and basic intensity of the ocean turbidity. The intent of the study was to explore how visible wavelength solar radiation is affected by its interaction with the regional environment. The work has operational significance because many types of military systems operate using visible wavelength energy and are greatly affected by scattering particles either airborne or suspended in the water column. The types of systems affected range from imaging and targeting to mine hunting and identification equipment.

THIS PAGE INTENTIONALLY LEFT BLANK

TABLE OF CONTENTS

I.	INTRODUCTION.....	1
A.	MOTIVATION	3
B.	OBJECTIVES	6
II.	THEORY.....	7
A.	MEASUREMENTS	7
B.	RADIATIVE TRANSFER	7
III.	DATA	15
A.	INSTRUMENT	15
IV.	PROCEDURES	19
A.	OVERVIEW.....	19
B.	REGIONAL METEOROLOGICAL OVERVIEW	19
C.	REGIONAL OCEANOGRAPHIC OVERVIEW.....	20
D.	METHODOLOGY	21
E.	LOCATIONS OF INITIAL ANALYSIS	23
F.	SPECIFIC ANALYSIS.....	25
V.	RESULTS AND DISCUSSION	27
A.	CASE STUDY DISCUSSION	27
1.	Case Study 1: April 15, 2001 (SeaWiFS file 2001 105 040236)	27
2.	Case Study 2: April 13 2001 (SeaWiFS file 2001 103 041557)	32
3.	Case Study 3: April 10, 2001 (SeaWiFS file 2001 100 034527)	37
4.	Regional Background Reflectance.....	41
5.	Experimental Algorithms	45
a.	<i>Airborne Dust Identifier</i>	48
i.	<i>Oceanic Turbidity Identifier</i>	54
VI.	CONCLUSIONS AND RECOMMENDATIONS.....	59
A.	CONCLUSIONS	59
B.	RECOMMENDATIONS.....	61
	LIST OF REFERENCES	63
	INITIAL DISTRIBUTION LIST	65

THIS PAGE INTENTIONALLY LEFT BLANK

LIST OF FIGURES

Figure 1.	SeaWiFS channels and their associated "colors".	2
Figure 2.	True color image of the study region from April 15, 2001, clearly showing the highly reflective Yangtze and Yellow river discharge.	5
Figure 3.	Wherli incoming solar radiation spectrum and associated SeaWiFS channels.	9
Figure 4.	Examples of reflectance spectra for varying air/ocean conditions.	10
Figure 5.	Examples of reflectance spectra for cloud and airborne dust.	11
Figure 6.	Reflectance at each pixel along the track line, from April 15, 2001.	13
Figure 7.	True color image from April 15, 2001, created with channels two, four and six as blue, green and red, respectively.	16
Figure 8.	True color image from April 15, with bathymetry overlay. Contour intervals are 10, 20 and 200 meters for yellow, red and blue, respectively.	22
Figure 9.	True color image from April 15, 2001, with the eight study locations depicted.	24
Figure 10.	Reflectance spectra from April 15, 2001 for each location and Rayleigh scatter.	28
Figure 11.	True color image from April 13, 2001, with the same eight study locations depicted.	33
Figure 12.	Reflectance spectra from April 13, 2001 for each location and Rayleigh scatter.	34
Figure 13.	True color image from April 10, 2001, with study locations depicted.	38
Figure 14.	Reflectance spectra from April 10, 2001 for clouds and dust.	39
Figure 15.	Minimum channel six reflectance (%) at each pixel for entire study period.	43
Figure 16.	Color composite using channels two, four and six for red, green and blue, respectively, from channel six minimization process. Also depicted are the seven study locations.	44
Figure 17.	Reflectance spectra for channel six composite process.	46
Figure 18.	Reflectance spectra of four study locations from April 15 and one location from April 10 (dust).	47
Figure 19.	True color image from April 15, with four study locations depicted.	49
Figure 20.	Image created from the dust identification algorithm for April 10.	50
Figure 21.	True color image from April 10, showing dust storm in upper right corner.	51
Figure 22.	Image created from the dust identification algorithm for April 15.	52
Figure 23.	True color image from April 15.	53
Figure 24.	Image created from the turbidity identification algorithm for April 15.	55
Figure 25.	True color image from April 13.	56
Figure 26.	Image created from the turbidity identification algorithm for April 13.	57

THIS PAGE INTENTIONALLY LEFT BLANK

LIST OF TABLES

Table 1.	SeaWiFS data files used in this study.	23
Table 2.	Primary study locations.	25

THIS PAGE INTENTIONALLY LEFT BLANK

ACKNOWLEDGMENTS

I would like to thank my advisor, Professor Philip A. Durkee, Department of Meteorology for his outstanding guidance and support, from the initial vision and throughout the development and completion of this thesis. His down to earth and patient personality, coupled with his realistic approach to the directions he provided, made my work easier and much more enjoyable. He knew when to work, when to play and when to say enough. I greatly respect and admire his character and this philosophy. I would also like to thank my co-advisor, Professor Steven R. Ramp, Department of Oceanography, for his insights and assistance in understanding the physical oceanographic characteristics of the study region. He contributed a significant oceanographic perspective to a meteorologically heavy topic. Kurt Nielsen deserves a special thanks for the numerous hours he spent assisting me with the computer programs used to analyze the data. Without his help, I would have been unable to accomplish this thesis in the time allotted.

My most sincere, heartfelt thanks go to LCDR David Ruth for helping me get through too many of the intense mathematics based courses here at the Naval Postgraduate School. He has a way of making the most difficult subjects understandable even for regular folks like me. He was truly one of my greatest instructors.

Lastly, but most of all, I would like to thank my wife Petra, who kept me from going insane during my first few quarters back in school and then sufficiently distracted me during our remaining time in Monterey. We got the most out of each day we had and it was an incredible tour. She is my best friend and with her I have had the best days of my life.

THIS PAGE INTENTIONALLY LEFT BLANK

I. INTRODUCTION

Space based observations have become an essential part of the scientific examination of the physical, chemical and biological properties of the earth's oceans, as well as an ever increasingly more valuable resource to examine the corresponding properties of the atmosphere. Additionally, the importance of these space-based sensors in understanding the earth's atmospheric and oceanic optical properties cannot be overstated. Using these sensors to perform analyses of specific regions of the earth is a vital part of accomplishing a complete and thorough survey of the environment in which the United States Armed Forces will be required to operate.

Remotely sensed visible wavelength imagery provides a means to closely examine the optical properties of both the ocean and atmosphere. The Sea-viewing Wide Field-of-view Sensor (SeaWiFS) is an exceptional device to perform such exploration. The SeaWiFS measures visible light in eight different wavelengths, ranging from 412 nanometers (nm) to 865 nm (Figure 1). The device has a pixel resolution of 1.1 kilometers (km), and can obtain measurements from 90% of the world's oceans in 2 days (NASA, 2001). Its high spatial resolution and relatively good temporal resolution allows for in-depth analysis of any ocean region. Using the data measured by the SeaWiFS, numerous products can be produced for use as stand-alone information sources or as input parameters for other programs. These products include data sets which can be analyzed pixel by pixel, such as: water leaving radiance for channels one through five, aerosol radiance for channels six and eight, pigment concentration, chlorophyll-a concentration, diffuse attenuation coefficient at channel three, epsilon value for the aerosol correction of channels six and eight, and the aerosol optical thickness at channel eight (NASA, 2001). After additional processing, two-dimensional mapped images of these products are also available. In addition to the products mentioned, numerous studies are currently in progress to develop new methods of extracting a wide variety of information from SeaWiFS data.

In addition to being able to "see" all of the world's oceans, even the coastal regions of hostile nations where access for in-situ measurements is denied, space-based

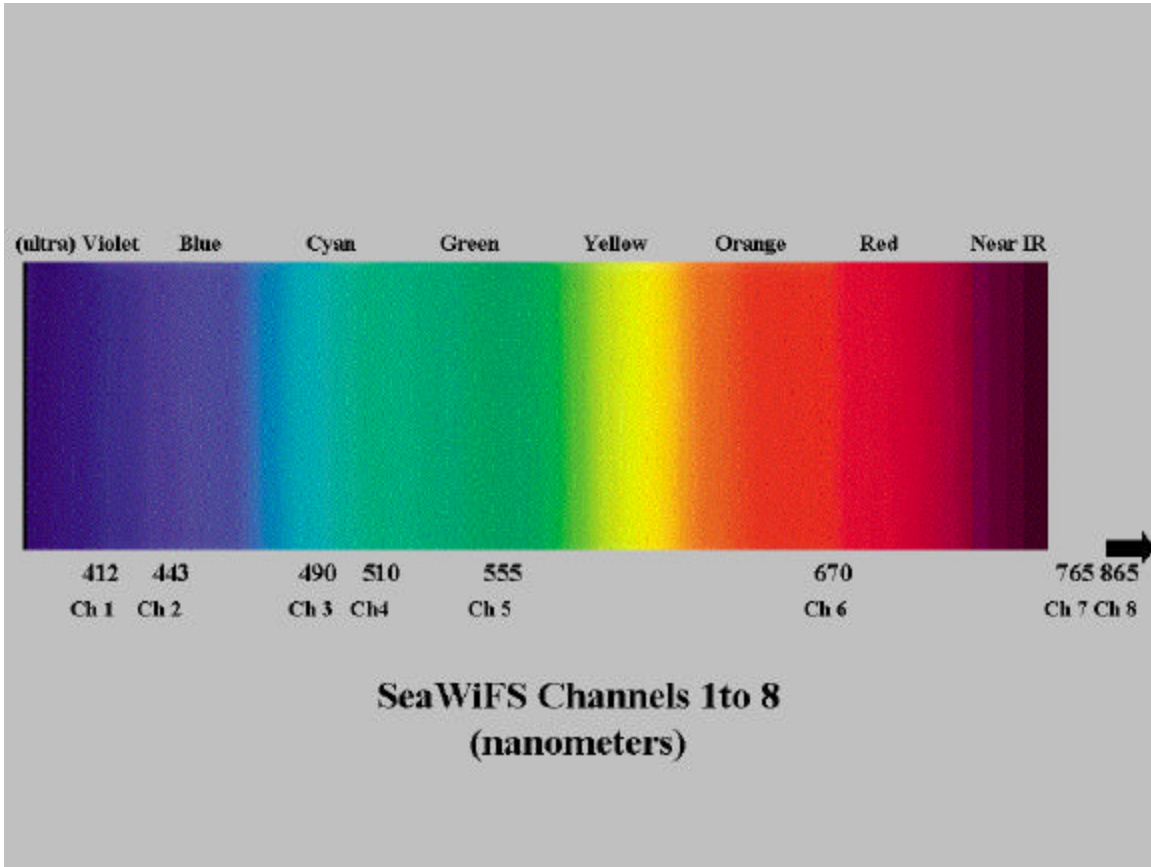


Figure 1. SeaWiFS channels and their associated "colors".

sensors will become increasingly more important as funding for in-theater observations and experimentation becomes more and more scarce. This is not to say that these sensors will allow for the suspension of in-situ measurements and observations. The requirement to compare and validate the results of any remotely sensed measurement will always exist. This is a necessary process that must be completed to ensure the accuracy of the data obtained.

A. MOTIVATION

In recent decades, the primary use of ocean color sensors, such as the Coastal Zone Color Scanner (CZCS), has been to characterize the geographic distribution and intensity of biological blooms and determine the chlorophyll concentration, sediment distribution and gelbstoffe concentrations (Clark, 1981). Sensors such as the CZCS have proven the value of spaceborne remote sensing. The new generation of sensors, such as the SeaWiFS and the Moderate-Resolution Imaging Spectroradiometer (MODIS), with their significantly higher resolution and greater number of measured wavelengths, will allow for even closer examination of the atmosphere and oceans.

The older generation sensors provided data for vast amounts of scientific analysis and discovery, however, with regard to military operations, ocean color sensors had not been heavily utilized. Currently, it is becoming more and more clear that these devices will allow for exceptional investigation of any part of the world. To date, their full potential has not been realized. Since the early nineties, there has been an ever-increasing focus on the importance of effectively conducting military operations in the littoral regions of the world. In order to complete these missions safely and effectively, it is essential that the operational environment be described and understood as accurately as possible. The optical properties of the theater of operations, both oceanic and atmospheric, are of the highest importance when planning and executing military operations. This is true because nearly every aspect of battle is affected by the state of the environment at the time of action. Two examples of environmental factors that can be described using information obtained from space borne sensors are aerosol optical depth and ocean turbidity.

The optical clarity of the atmosphere affects everyone from airborne flight crews to look outs aboard ships, and the optical clarity of the ocean affects the operations of surface and subsurface crews. Without going into detail on any specific weapons system, it should be made clear that any system relying on visible wavelength radiation to perform its functions will be affected by the scattering particles present in the path of the radiation. The types of systems in this category range from imaging and targeting to mine hunting and classification equipment. In the atmosphere, airborne dust particles will cause scattering of the radiation resulting in decreased image quality and effective sensor range. In the ocean, suspended particles will cause a similar scattering affect. Mine hunting and classification is an excellent example of one area of operations that are adversely affected by high ocean turbidity. Laser line scan systems use radiation in the 400 to 600 nm range. Their performance relies on the ability to send and receive visible light and it is certainly affected by the scattering caused by suspended particles in the water column.

Highly turbid water also impacts the accuracy of aerosol optical depth retrievals. Currently, most optical depth programs consider the water surface to be a zero or at least known reflectance. If a reflectance value is known, it is usually a very small number on the order of 0.005 and does not change with geographic location. One glance at a region containing high turbidity water will prove that the use of a zero reflectance value in these regions is not accurate. Figure 2 is an image of the East China Sea region. In this image the Yangtze River discharge is clearly visible. The problem this creates is due to the increased oceanic reflectance in highly turbid regions. These areas reflect a far greater amount of visible wavelength energy and cause the aerosol optical depth programs to either grossly over-estimate the optical depth of the associated region or mask the region as cloud covered. This deficiency in the aerosol optical depth programs can be misleading to analysts if it is not completely explained or understood.

The examples discussed above are but two of the numerous subjects that can be examined with data retrieved by spaceborne sensors. Along with this increased attention to the littoral regions, has come an increased desire to extract more and more information from these available sensors. Sensors currently in orbit, such as the SeaWiFS, are one of the best ways to get information on a wide variety of the theater's physical properties

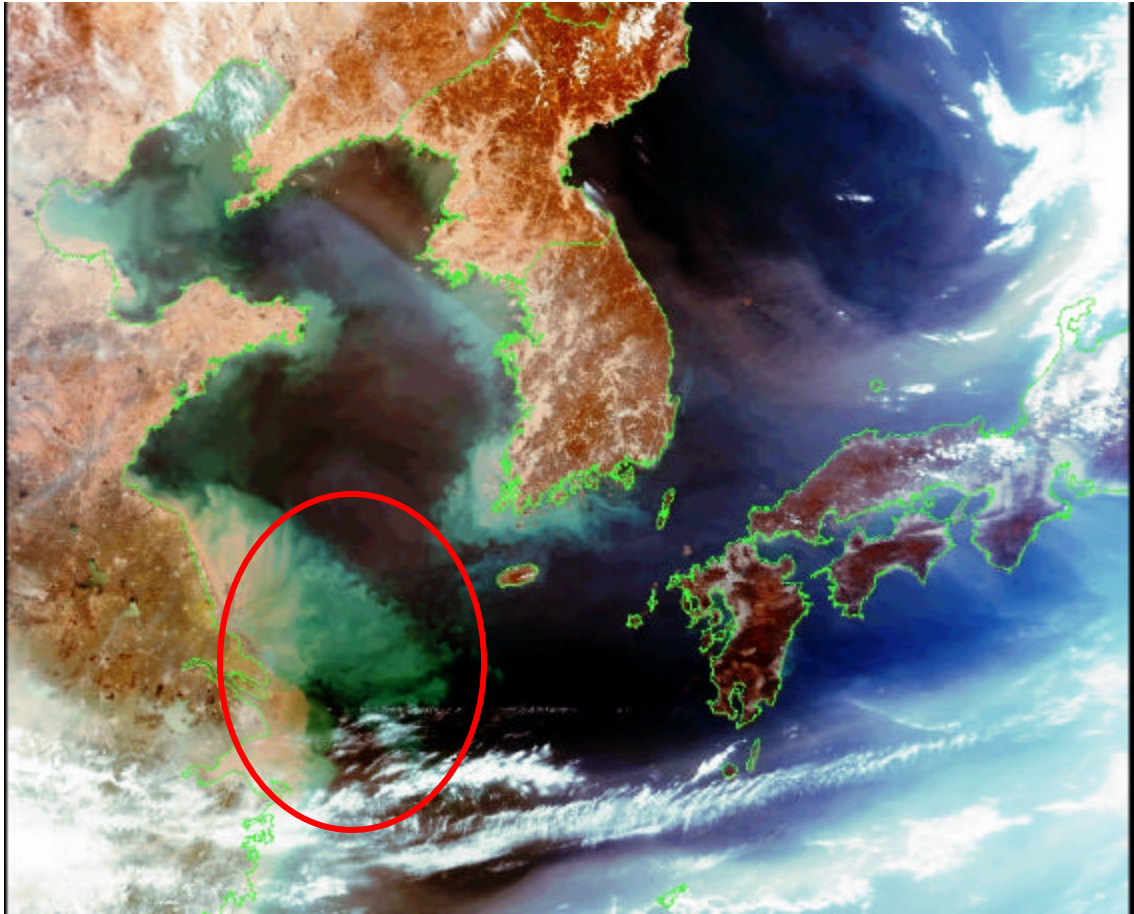


Figure 2. True color image of the study region from April 15, 2001, clearly showing the highly reflective Yangtze and Yellow river discharge.

including: cloud cover, aerosol optical depth, biological activity, the location of oceanic fronts and ocean turbidity.

B. OBJECTIVES

The object of this thesis was to perform an area study of the region encompassing the East China Sea, the Yellow Sea and the Sea of Japan, focusing on the characteristics of the oceanic and atmospheric optical properties. There were three primary oceanographic conditions and four primary atmospheric conditions studied. The oceanographic conditions included 1) very clear, low turbidity water, such as that of the Sea of Japan east of North Korea, 2) water of medium turbidity and/or water with significantly altered color, as compared to surrounding water, such as the water off the coast of the southern South Korea or the extended Yangtze River plume, and 3) very high turbidity water, such as that located directly seaward of the Yangtze River Mouth and along the associated Chinese coastline. The atmospheric conditions included the following 1) clouds, 2) haze of a blue tint, 3) haze of a brown or red tint, and 4) areas experiencing obvious airborne dust events, such as the dust storm of April 10, 2001.

The source of the analysis data was the measurements collected by the SeaWiFS device during the spring of 2001. The SeaWiFS radiance measurements obtained during the Aerosol Characterization Experiment-Asia (ACE-Asia) were examined and the unique spectral characteristics of differing oceanic and atmospheric conditions were identified. Using the information obtained from the spectral analysis, experimental algorithms were developed to isolate atmospheric or oceanic properties, ranging from clouds and airborne dust to sediment laden, high turbidity ocean regions. Using these algorithms, it is possible to produce regional images that expose the geographic distribution and basic intensity of the features of interest. The possible products that could be produced from these algorithms range from cloud masks and dust identifiers to ocean turbidity distributions and qualitative turbidity estimates. A second objective of the study is to develop a method to determine the base background reflectance of the regional seas. The purpose for this effort is to improve the input parameters for existing aerosol optical depth models in order to enhance their performance.

II. THEORY

A. MEASUREMENTS

The SeaWiFS, flying onboard the OrbView-2 spacecraft, is one of the latest calibrated and validated space borne sensors designed to retrieve ocean color information. Spaceborne sensors, such as the SeaWiFS, retrieve global radiance measurements, which can be used for numerous commercial and operational applications. Specifically, they are well-suited for providing high resolution radiance measurements that allow scientists and researchers to determine vast amounts of information about the optical properties of the oceanic and atmospheric environment of interest. The measurements used in this study were compiled during ACE-Asia, in the spring of 2001, and consisted of approximately sixty SeaWiFS overpass data sets. Ultimately, only the nine best data sets were used, as will be described in the next chapter. The SeaWiFS data was downloaded and stored during the experiment at a ground site set up by the Naval Postgraduate School at Marine Corps Air Station Iwakuni, Japan.

B. RADIATIVE TRANSFER

Before any scientific study using data retrieved by a space borne sensor can begin, an understanding of the basic physics of radiative transfer is essential. The sensor, flying on board the satellite or spacecraft, "sees" the electromagnetic energy that leaves the top of the atmosphere at varying wavelengths. Prior to leaving the atmosphere, the electromagnetic energy can encounter a number of physical processes that can alter its final intensity as it enters space, after which, it remains essentially unchanged for the rest of the journey to the sensor. While still in the atmosphere, photons can be scattered, absorbed, transmitted, and emitted. The radiation that ultimately reaches the sensor is a combination of scattered or reflected solar radiation off the earth's surface, clouds and atmospheric aerosols, or radiation emitted from terrestrial sources. The SeaWiFS measures radiation in the visible spectrum between 412 and 865 nanometers, in which there are few significant terrestrial sources, so all measured radiation is from scattered or

reflected solar radiation. Figure 3 depicts the average incoming solar radiation in the visible part of the spectrum (Wherli, 1985).

Figures 4 and 5 depict examples of typical spectral reflectance profiles for various combinations of water turbidity and atmospheric aerosols. The physical properties of differing substances and materials, which create the unique spectral reflectance signature, are also what cause all things to have their "color," as perceived by the human eye. Stating that something has a specific color is not scientifically precise. The color perceived by the human eye is actually the result of the distribution of absorption versus reflectance of all visible light incident on an object. Because all matter reflects the visible wavelengths in unique proportions, it is possible to carry out meaningful scientific research by analyzing the received reflectance spectrum of differing atmospheric and ocean phenomenon.

As alluded to earlier, there are three possible responses that may take place when a photon impacts any medium. These are transmittance, absorption, and reflectance, and different substances cause different responses. Every material or substance has unique characteristics, with regard to how it affects incoming electromagnetic energy. For example, within the visible portion of the electromagnetic spectrum, a liquid water surface reflects 400 to 550 nm energy poorly and becomes even more absorptive as the wavelength increases, toward 600 to 865 nm. A spectrum created from reflected solar radiation off of clean water would decrease from 400 to 865 nm (Figure 4). Clouds, unlike liquid water, reflect all wavelengths well and more evenly than a water surface, so a spectrum from the solar radiation reflected off clouds would appear flatter, decreasing slightly from 400 to 865 nm (Figure 5). Airborne dust reflects all wavelengths more evenly than clouds and the spectrum is usually very flat. Although dust reflects all wavelengths relatively equally, the wavelengths in the 550 to 750 nm range are slightly elevated and cause the dust to appear tan or brown in color (Figure 5). A very turbid ocean has a spectrum that reveals relatively even reflectance across most of the visible spectrum and then falls sharply beyond 670 nm due to strong water absorption (Figure 4, green line). Atmospheric aerosols can cause more subtle changes in the reflected radiation. For example, an atmospheric haze created by very tiny pollution particles, which usually appears blue, will increase the reflectance of the 400 to 500 nm

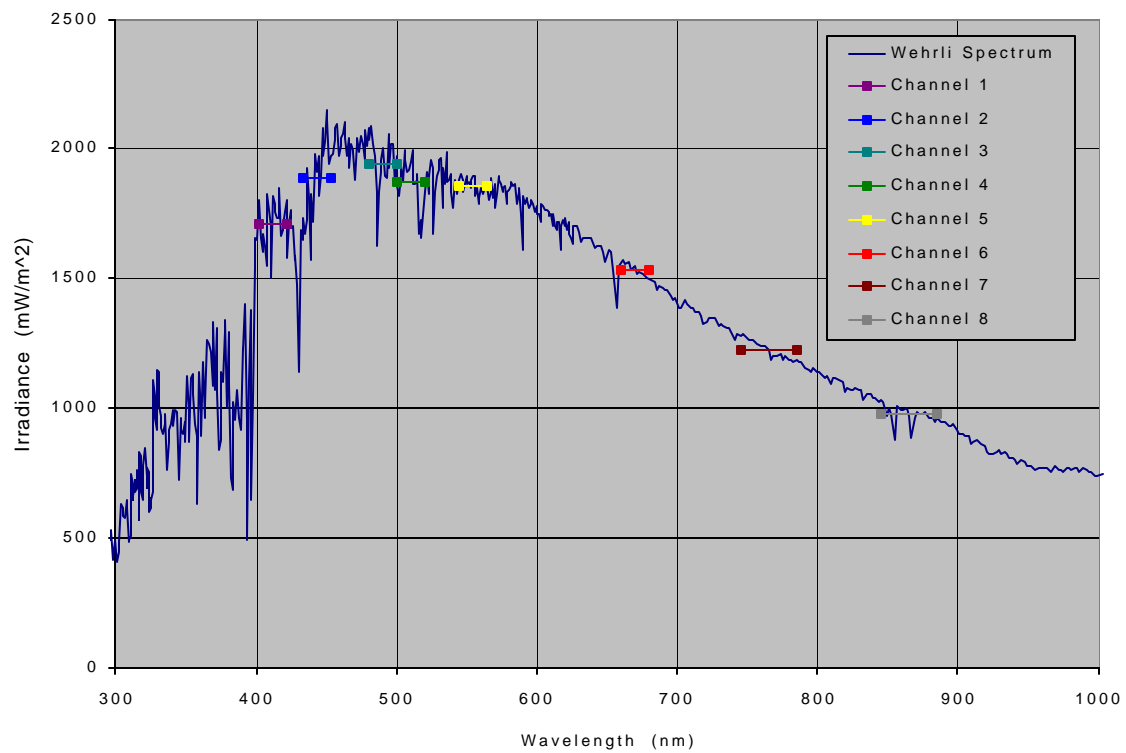


Figure 3. Werhli incoming solar radiation spectrum and associated SeaWiFS channels.

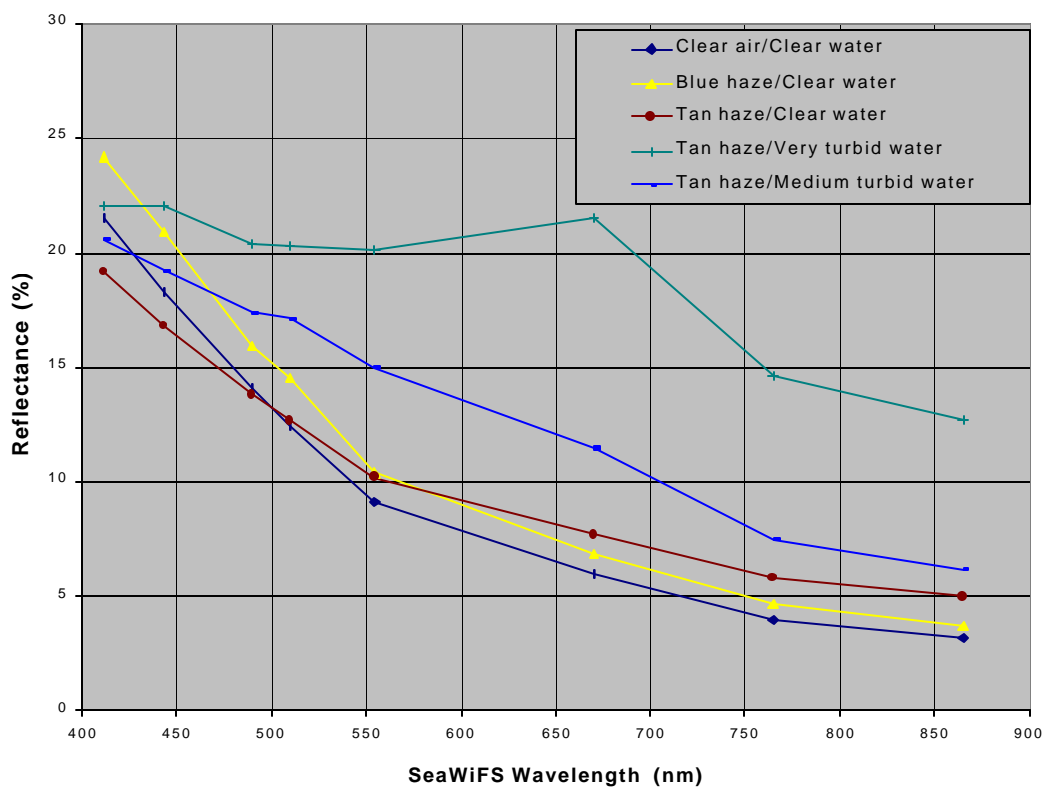


Figure 4. Examples of reflectance spectra for varying air/ocean conditions.

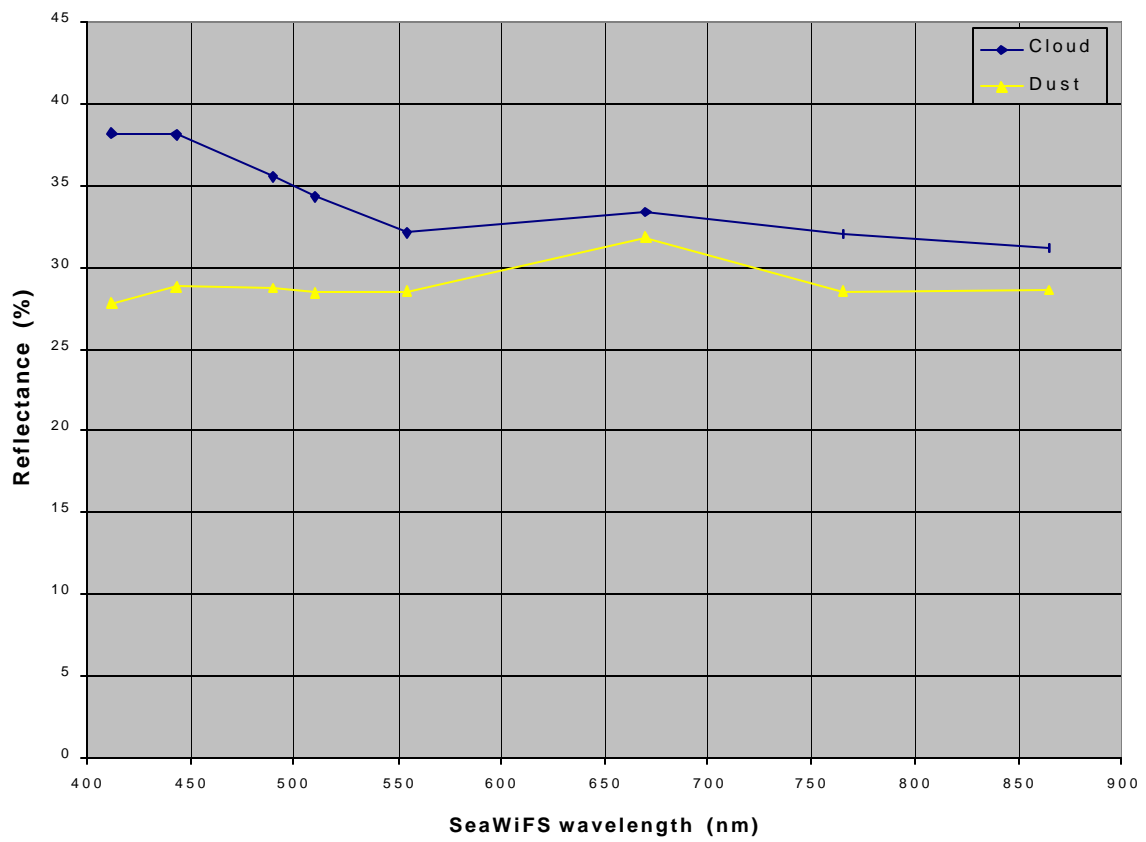
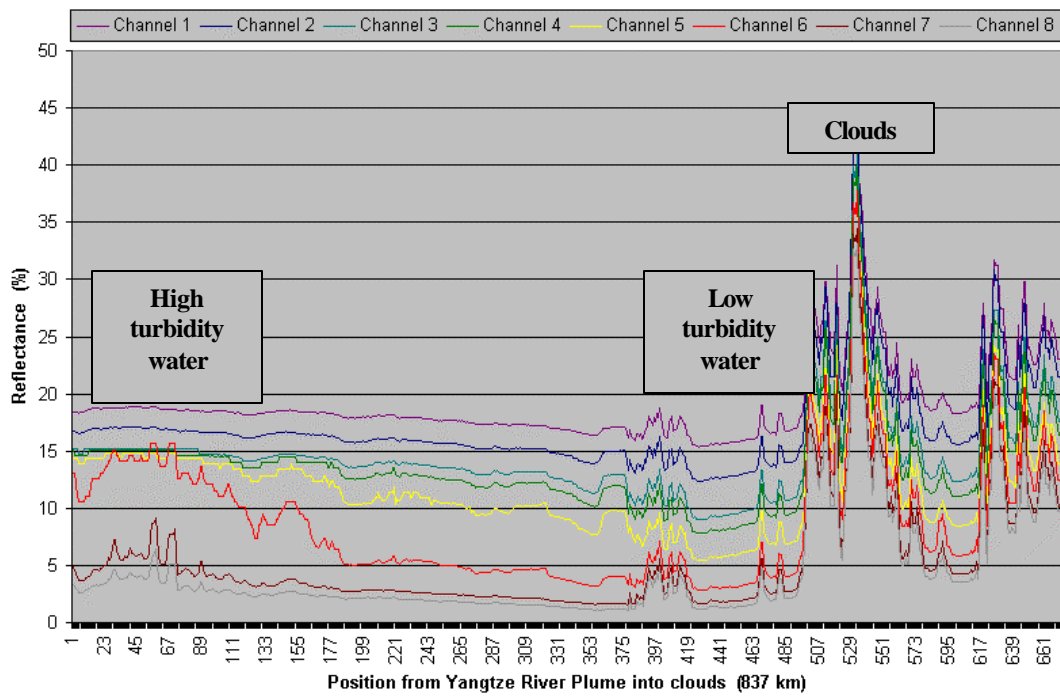


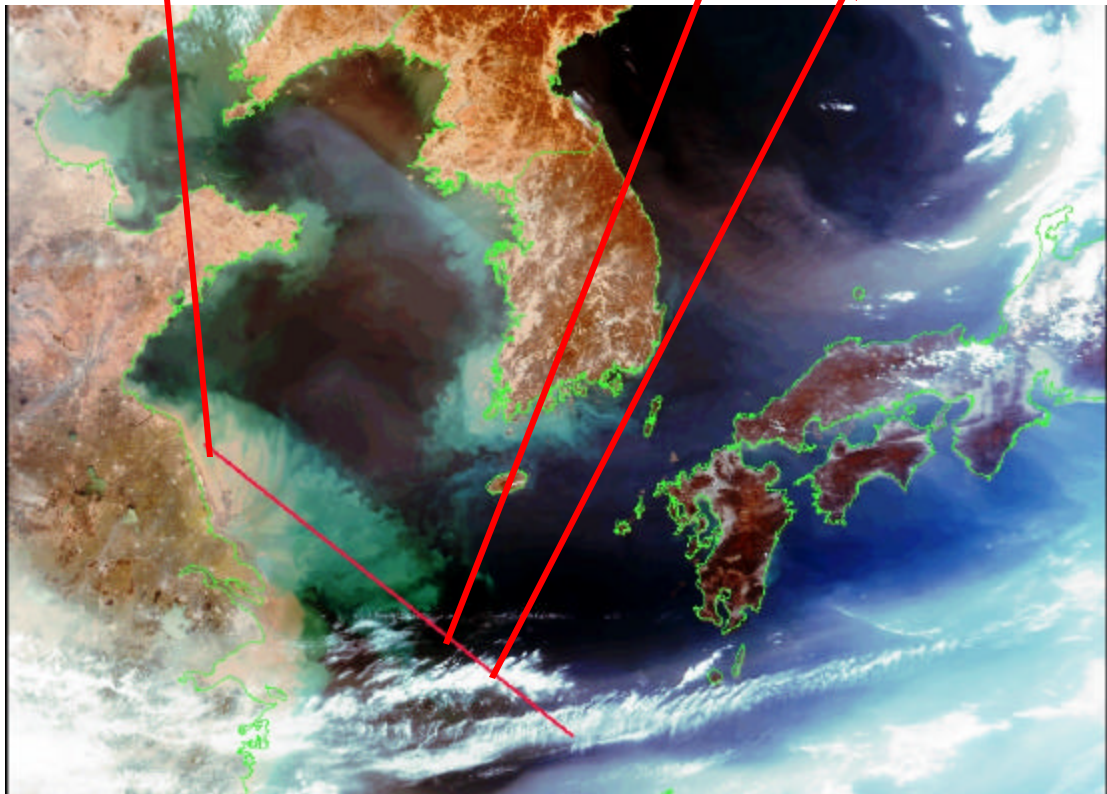
Figure 5. Examples of reflectance spectra for cloud and airborne dust.

wavelengths, regardless of the primary background signature. A haze created by larger particles, usually from tan to brown in color, will reflect more of the 550 to 750 nm wavelengths.

Figure 6(a) shows the reflectance received as a function of wavelength from each pixel along the track line depicted on the true color SeaWiFS image in Figure 6(b). This track line crosses through a variety of atmospheric and oceanic conditions and the associated changes in reflectance can be examined. In this example, the highly turbid water at the northwest end of the track reflects a proportionally greater amount of the longer wavelengths and thus appears brown in color, as compared to the dark blue of the low turbidity water. Clouds reflect all visible wavelengths well and therefore the associated reflectance is both greater and more nearly equal across all wavelengths. This is an example of how the received reflectance changes depending on the environmental conditions at the point of interest. This principle of unique reflectance is the heart of this thesis.



(a)



(b)

Figure 6. Reflectance at each pixel along the track line, from April 15, 2001.

THIS PAGE INTENTIONALLY LEFT BLANK

III. DATA

In order to achieve the objectives of this thesis, it was necessary to review all of the SeaWiFS data obtained during the Ace-Asia timeframe and identify suitable cloud-free days, which coincided with satellite overpasses centered on the area of interest. This was accomplished by reviewing each overpass data set, correcting the navigation to align with coastline overlays, and viewing a true color image made from combining channels two, four, and six, which correspond to blue, green, and red wavelengths, respectively. Figure 1 depicts the measured SeaWiFS channels, wavelengths and colors. By creating an image associating blue to the channel two reflectance, green to channel four and red to channel six, it was possible to qualitatively determine the general environmental conditions at the time of the sensor overpass. Figure 7 is an example of a true color image created this way. Using this procedure, it was possible to ensure that the chosen data sets contained the unique oceanic or atmospheric features of interest and contained a minimum amount of cloud cover. This chapter will describe the data sets and the sensor used in this study.

A. INSTRUMENT

The SeaWiFS, flying onboard the OrbView-2 spacecraft, is an eight-channel, passive, visible light radiometer that measures scene radiance at 412, 443, 490, 510, 555, 670, 765, 865 nm (Figure 1), and is one of the latest calibrated and validated space borne sensors designed to retrieve ocean color information. The bandwidth is 20 nm for channels one through six and 40 nm for channels seven and eight. The actual “color” of these wavelengths ranging from ultra violet to dark red (near infrared), from shortest to the longest wavelengths respectively. The data can be easily examined in either the original radiance form or as reflectance, with a simple mathematical correction applied, which accounts for the solar constant per wavelength and zenith angle. The OrbView-2 spacecraft carrying the SeaWiFS operates in a sun-synchronous, descending node, polar orbit, approximately 705 kilometers (km) above the earth’s surface. By virtue of its polar orbit, close to the earth, the sensor is capable of producing 1.1 km spatial resolution

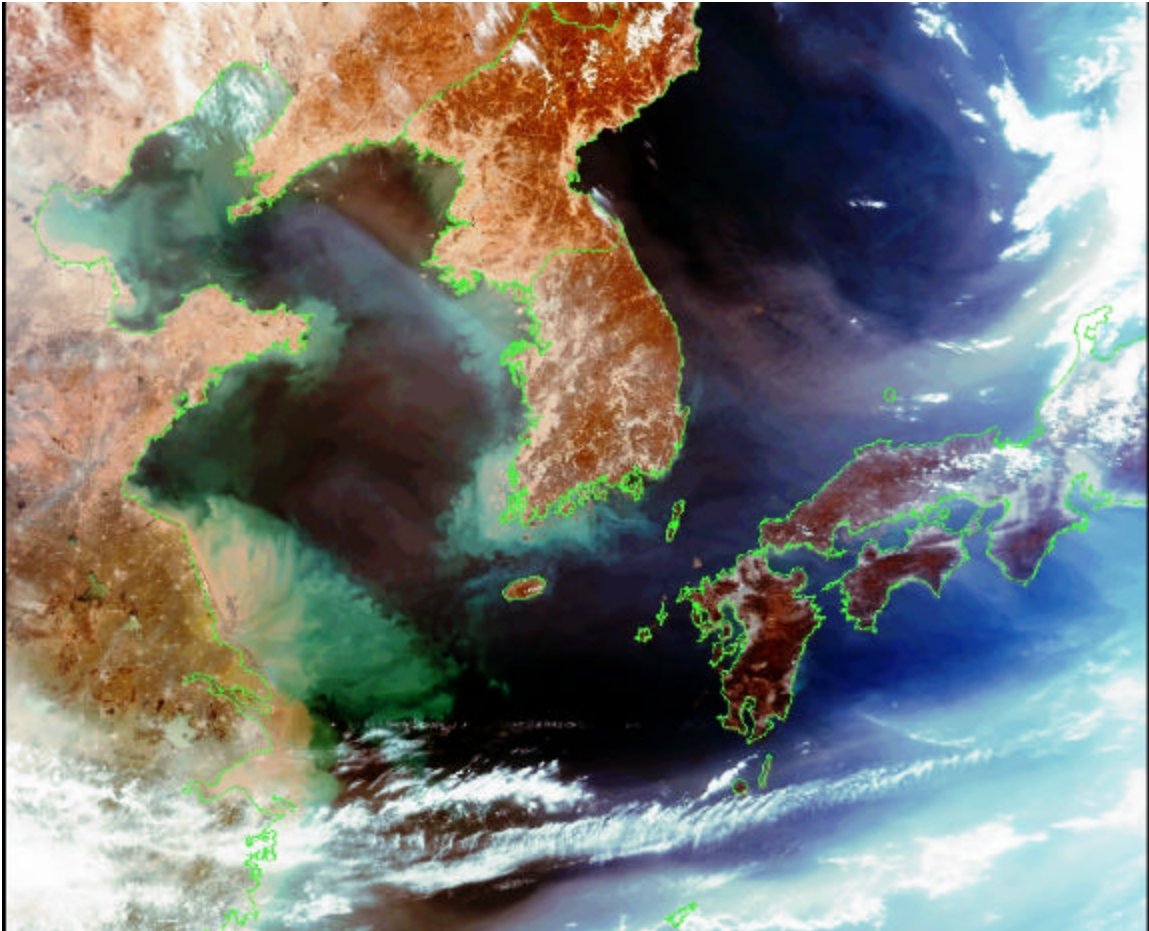


Figure 7. True color image from April 15, 2001, created with channels two, four and six as blue, green and red, respectively.

imaging in the Local Area Coverage (LAC) mode. In the Global Area Coverage mode (GAC), the resolution of the sensor is 4.5 km per pixel (NASA, 2001). The trade off to high spatial resolution is lower temporal resolution. The SeaWiFS, however, can still obtain imagery of 90% of the worlds oceans in 2 days. When retrieving information in the LAC mode, a limited coverage rate is available, and an increased download rate is required. The data is ultimately available in 10 bit digitization raster files. The foundation of this thesis is the retrieved LAC data focusing on the Sea of Japan, the Yellow Sea and the East China Sea during the ACE-Asia time frame.

The new generation of sensors will allow for wide-ranging advances in scientific research. Unlike the preceding sensors, which only measured one or two wavelengths, these sensors have the capability to measure multiple wavelengths within the visible spectrum. The great benefit from this multi-channel ability is that the retrieved individual spectral signature, for a specific geographical location, can be used to identify differing atmospheric and oceanic conditions. This process is analogous to fingerprinting, due to the unique spectral response of different atmospheric and oceanic constituents. The major emphasis of this work was to accurately characterize the spectral signatures of the received radiance and/or reflectance from varying locations.

THIS PAGE INTENTIONALLY LEFT BLANK

IV. PROCEDURES

A. OVERVIEW

SeaWiFS measurements allow for the in-depth analysis of the reflected solar energy in eight visible wavelengths. By examining the spectral signature of the reflected visible light, certain characteristics can be identified for differing oceanic and atmospheric states that are unique to the physical conditions at the time of the measurement. Following this premise, an investigation was performed to identify the spectral signature of these different oceanic and atmospheric combinations. Once the unique characteristic of the spectral signature was identified for a specific air/ocean combination, attempts were made to develop mathematical algorithms, using ratios of different wavelength reflectance, which would expose the feature of interest. By running the successful algorithms on overpass data, it is possible to produce images that depict the geographic extent and qualitative intensity of the isolated oceanic or atmospheric feature.

Additionally, during the process of examining the data, continual observation was made to identify a method to best isolate the background reflectance of the entire region. The goal of this last effort was to develop better input parameters for the SeaWiFS aerosol optical depth algorithm currently in use. By determining regionally specific reflectance values, as opposed to using the same zero reflectance value for all geographic areas, it would be possible to improve the overall accuracy of the program.

B. REGIONAL METEOROLOGICAL OVERVIEW

This thesis is intended to contribute to future improvements in various meteorological products. It must be noted that much of the meteorological descriptions contained within this document will be explained in a very basic manner. It is not necessary to go into the details of how specific events came to pass, only that the current optical state of the event studied is fully explained.

In general, the prevailing weather patterns remained constant throughout the study period, consisting of an eastward traveling jet that moved the frontal systems across the

region. During much of the period, there was a southerly component to this persistent eastward motion. Traveling east with these weather systems was a tremendous amount of pollution aerosol and dust. The make up of this pollution aerosol is the focus of numerous ongoing experiments and studies as part of the ACE-Asia project. It is known, however, that a major portion of this pollution is industrial exhaust, smoke and soot being transported out of China. The source of the dust in the atmosphere across the region is being intensely studied as well, but it is likely that most of it comes from the Gobi Desert. There were no entirely cloud free days. In most cases the cloud cover was approximately 50 percent. The study locations were not all visible on every overpass chosen. The overpasses were chosen in order to maximize the cloud free area over the study locations. In every image studied, there were regions containing haze that varied in both distribution and intensity. In the true color images produced, the haze ranged in color from light blue to brownish red. Heavy dust events showed up tan to brown in these images. Within the nine overpasses chosen for examination, there were numerous meteorological events available to focus on. The locations of interest were chosen to sample a variety of these events, but by no means cover all of the possibilities.

C. REGIONAL OCEANOGRAPHIC OVERVIEW

The study region is composed of a number of interconnecting seas. These include the Sea of Japan, the Bohai Sea, the Yellow Sea, the East China Sea and the Philippine Sea. The geographic locations chosen for analysis represented all but the Bohai Sea. Both the Sea of Japan and the Philippine Sea are deeper than 2000 meters over most of their area and are normally the clearest waters in the region. The Bohai Sea, Yellow Sea and the broad continental shelf of the East China Sea are all less than 100 meters in depth. The deep basin north of the Ryukyu island chain exceeds 2000 meters depth. The most significant impact to these seas is the input from the Yellow River into the Bohai Sea and the Yangtze River into the East China Sea. The sediment transport into the region from these two rivers is enormous. The sediment transport from the Yellow River into the Bohai Sea is the second greatest of any of the world's rivers, 1.4 billion metric tons per year (Beardsley *et al*, 1985) and the Yangtze River sediment discharge into the East China Sea is estimated to exceed 142 million cubic meters annually (NASA,

Geomorphology from Space, Goddard Space Flight Center, Distributed Active Archive Center, 2001). The Yellow Sea gets its name from this discharge. Historically, the Yellow River has alternated between flowing into the Yellow Sea and or into the Gulf of Bohai. Currently, it flows to the north into the Gulf of Bohai. The sediment fan created in the East China Sea by the discharge from the Yangtze River and the numerous small rivers along the northern coastline is an amazing site in visible imagery. In Figure 7, a true color composite of the region, this outflow fan can be seen in the lower left corner of the image. The sediment fans out into the East China Sea and the Yellow Sea and stands out in any cloud free image. The Yangtze River discharge is the most sediment-laden water in the East China Sea region and much of it is confined to the coast and moves southward. However, the smaller rivers to the north of the Yangtze provide a significant amount of the sediment that creates the portion of the fan that is propagated out into the central East China Sea. This sediment is transported off the coast by a shallow, low salinity layer that is propelled by off shore flow from the Jiangsu region (Beardsley *et al*, 1985). A bathymetric feature of interest in the East China Sea is the Yangtze Bank, a shallow region that follows the 50-meter isobath and extends out from the mouth of the Yangtze River towards the southeast, extending past 125 degrees east longitude. Figure 8 shows the bathymetry of the region overlaid on a true color image. This bank is very interesting because the highly visible sediment fan disperses out in a pattern remarkably similar to the shape of the bank. It is not clear, whether sediment deposition is an element in the formation of this bank. It is possible that the noticeable turbid water fan to the east of the Yangtze River mouth could also be caused by sediment re-suspension from the shallow Yangtze Bank. The area in which this turbid water fan covers seems to be remarkably consistent, regardless of the weather at the time of imaging. This may indicate that re-suspension is less likely, but certainly does not provide enough evidence to make any firm conclusions.

D. METHODOLOGY

As discussed in the previous sections, the SeaWiFS overpasses chosen for examination were the ones that were centered best on the East China Sea region and were, to the largest extent, cloud free. The procedure used to examine the data available

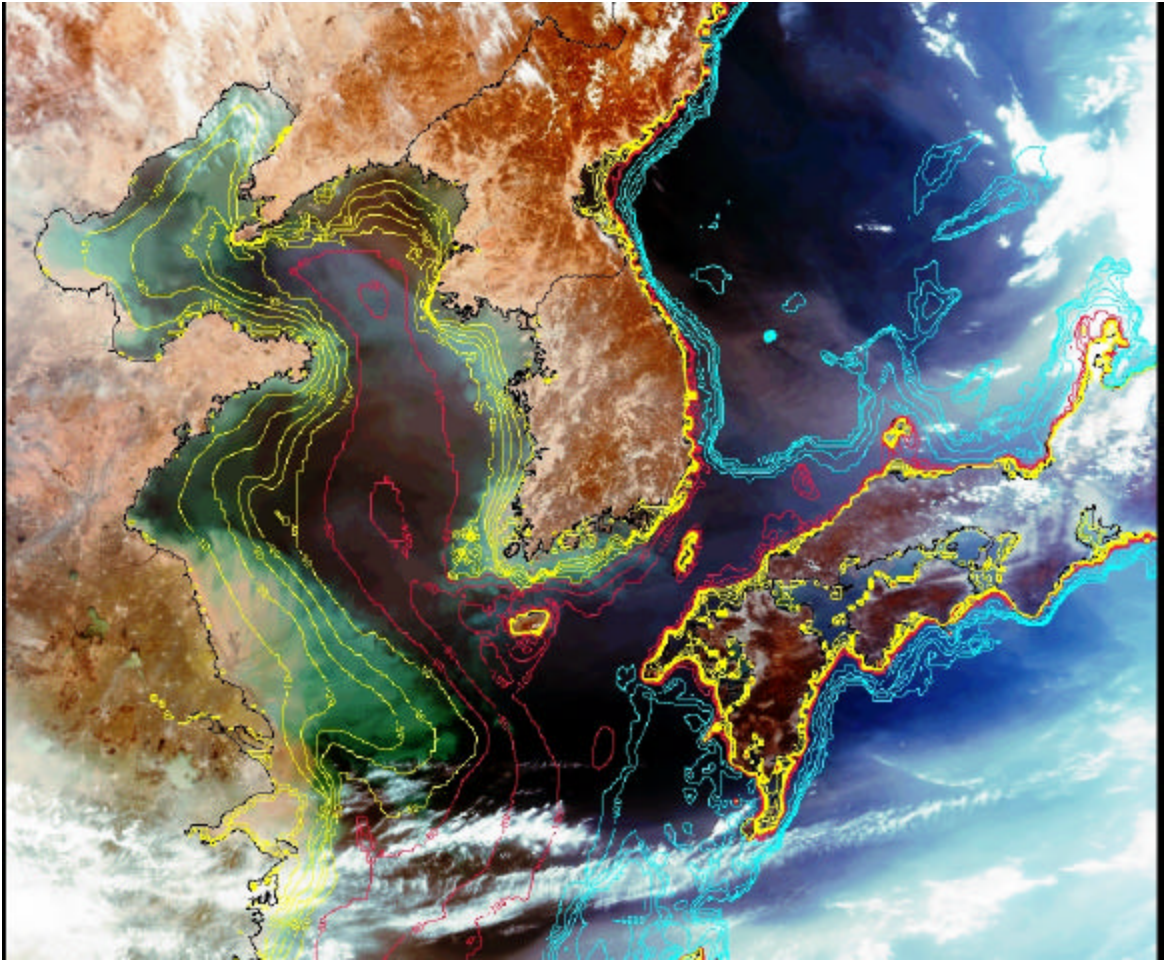


Figure 8. True color image from April 15, with bathymetry overlay. Contour intervals are 10, 20 and 200 meters for yellow, red and blue, respectively.

from each of these overpasses was essentially the same. A true color image was produced to aid in the initial detection of atmospheric or oceanic characteristics of interest. Initially, eight geographic locations were chosen as study points. These points were picked in a manner that would ensure all of the desired oceanic or atmospheric conditions would be represented. Recall, the three primary oceanic conditions included 1) very clear, low turbidity water, such as that of the Sea of Japan east of North Korea, 2) water of medium turbidity and/or water with significantly altered color, as compared to surrounding water, such as the water off the coast of the southern South Korea or the extended Yangtze River plume, and 3) very high turbidity water, such as that located directly seaward of the Yangtze River Mouth and along the associated Chinese coastline. The atmospheric conditions included the following 1) clouds, 2) haze of a blue tint, 3) haze of a brown or red tint, and 4) areas experiencing obvious airborne dust events.

The SeaWiFS overpasses that provided the largest amount of cloud free area and were centered on the desired region are shown in Table 1.

Day	Month	Year	Julian Day	Time (UTC)
10	April	2001	100	03:45:27
12	April	2001	102	03:33:03
13	April	2001	103	04:15:57
14	April	2001	104	03:20:34
15	April	2001	105	04:02:36
16	April	2001	106	03:03:20
19	April	2001	109	03:37:12
26	April	2001	116	03:41:12
27	April	2001	117	04:24:40

Table 1. SeaWiFS data files used in this study.

E. LOCATIONS OF INITIAL ANALYSIS

The eight regional locations chosen for the initial analysis are identified in Figure 9, a true color composite image, and are listed in Table 2.

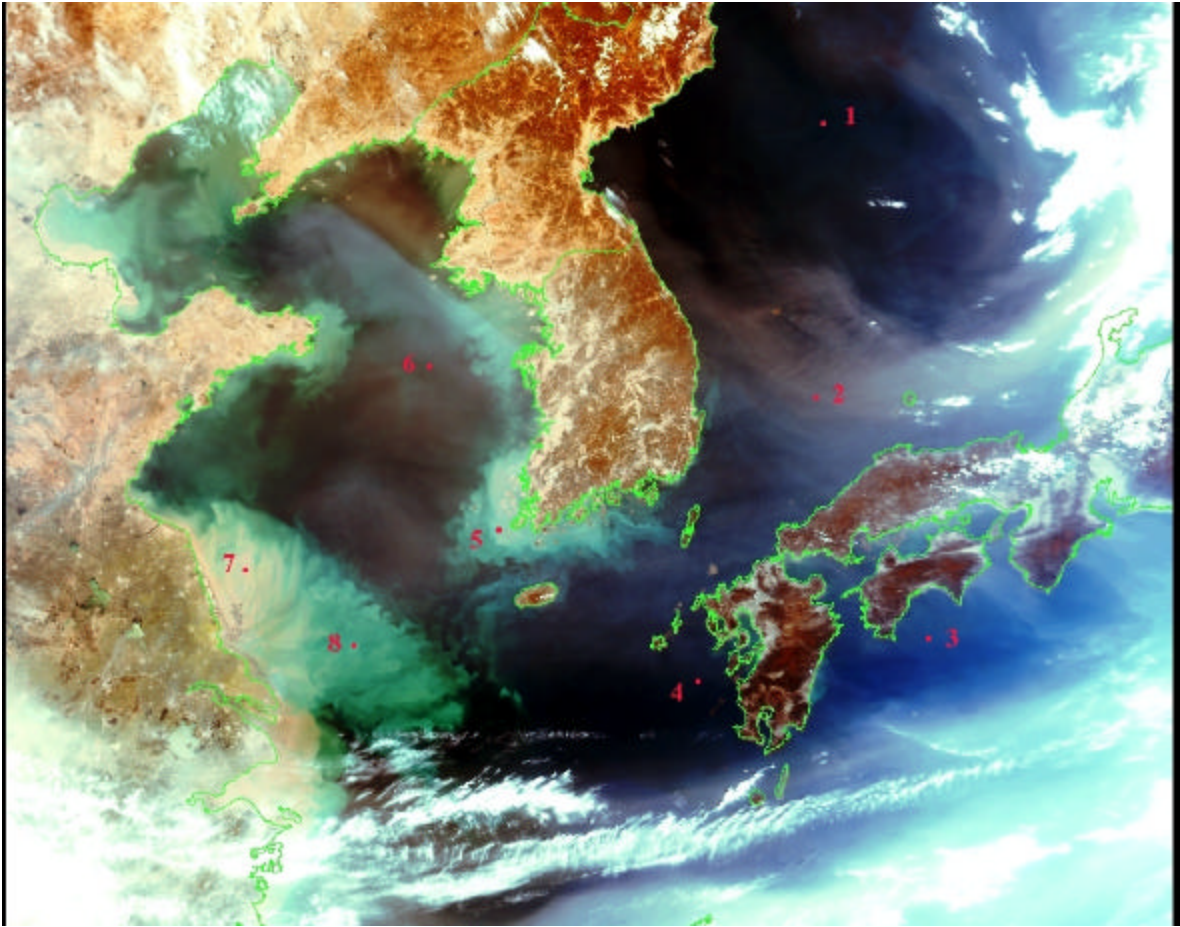


Figure 9. True color image from April 15, 2001, with the eight study locations depicted.

Point	Latitude	Longitude	Geographic Location	Water type
1	40 05.17 N	131 42.00 E	Central Sea of Japan	Very clear, dark blue
2	36 15.56 N	131 34.34 E	Southern Sea of Japan	Very clear, dark blue
3	32 44.26 N	133 36.83 E	Philippine Sea	Very clear, dark blue
4	32 05.48 N	129 26.75 E	Eastern East China Sea	Very clear, dark blue
5	34 22.08 N	125 52.39 E	Eastern Yellow Sea	Very turbid, sediment laden
6	36 42.23 N	124 38.39 E	Central Yellow Sea	Very clear, dark blue
7	33 46.15 N	121 18.06 E	Western Yellow Sea	Very turbid, sediment laden
8	32 38.89 N	123 16.73 E	Eastern East China Sea	Medium turbid, sediment laden

Table 2. Primary study locations.

Points one thru four are located in regions of typically very clear dark blue water. Point 5 is located in a region of high land run off and is typically very turbid water. Point six is located in a region of relatively clear water, dark blue water. Point seven is located in the middle of the Yangtze River outflow and is the most sediment heavy, turbid water in the region. Point eight is located in the extended Yangtze River outflow fan and exhibits characteristics of more settled turbidity water and/or altered ocean color due to colored dissolved organic matter (CDOM). The amount and intensity of the overlying atmospheric haze varied at each location during the study period.

F. SPECIFIC ANALYSIS

Once the overpasses and study locations were determined, the spectral signatures for each location were produced, compared to the true color image of the atmospheric and oceanic events at the time, and analyzed for distinguishing features. For each overpass, the SeaWiFS data was converted from radiance to reflectance. This is a relatively simple calculation that accounts for the varying, wavelength dependent, magnitude of incoming solar radiation (Figure 3) and the solar zenith angle. Once the data for each of the nine suitable days had been converted to reflectance, the point measurement for each of the eight wavelengths was recorded for each location. By plotting these reflectance values against the corresponding wavelength, a spectrum was produced and then was analyzed for distinguishing features. For most over water locations examined, the measured reflectance decreased from shorter to longer wavelength. This decrease in reflectance with increasing wavelength is because water is

a better absorber of the longer wavelengths. As the constituents of the atmosphere and/or the ocean change, the amount of absorption and reflection also change. These changes in the spectrum, caused by the differing properties of the ocean or the atmosphere, are what allow the identification of typical signatures for individual combinations of oceanic and atmospheric properties.

V. RESULTS AND DISCUSSION

A. CASE STUDY DISCUSSION

The following three cases were found to best describe the results of the study completed. All of the seven identified features of the atmosphere and ocean are represented in these three cases. In each case, the unique features of the measured reflectance spectrum from each location will be examined. Once the discussion of the individual points is completed, a discussion of the method used to determine baseline regional background reflectance values and their uses will be presented. Lastly, an explanation of proposed algorithms and their uses will be presented.

1. Case Study 1: April 15, 2001 (SeaWiFS file 2001 105 040236)

Figure 9 shows a true color image of the region with the study locations identified. Figure 10 depicts the measured reflectance at the eight original locations as a function of wavelength. In order to establish the unique spectral characteristics of each location's atmospheric and oceanic state, the spectral profile of reflectance per wavelength was examined and compared to the true color composite. Each point will be discussed and the spectral characteristics identified.

The spectral profile from point 1, located over very low turbidity water and under a very low haze atmosphere, shows a relatively smooth, exponential drop in reflectance, as wavelength increases. The shape of this profile is representative of the curve created by Rayleigh scattering and the scattering from liquid water. Rayleigh scatter takes place when the radius of the scattering particles is much smaller than the incident wavelength. For the visible wavelengths, this size parameter corresponds to the size of individual molecules of the atmospheric constituents, particles on the order of 10^{-3} micrometers. The molecules that make up the air in the atmosphere scatter light in the visible spectrum greatest in the ultra-violet, 400 nm, and progressively less as you move across the spectrum toward the longer wavelengths of red and near infrared, 670 to 865 nm. This curve has the approximate shape of $1/\lambda^4$, with regard to how much reflectance is measured per wavelength. The dotted red line on Figure 10 depicts a Rayleigh scattered

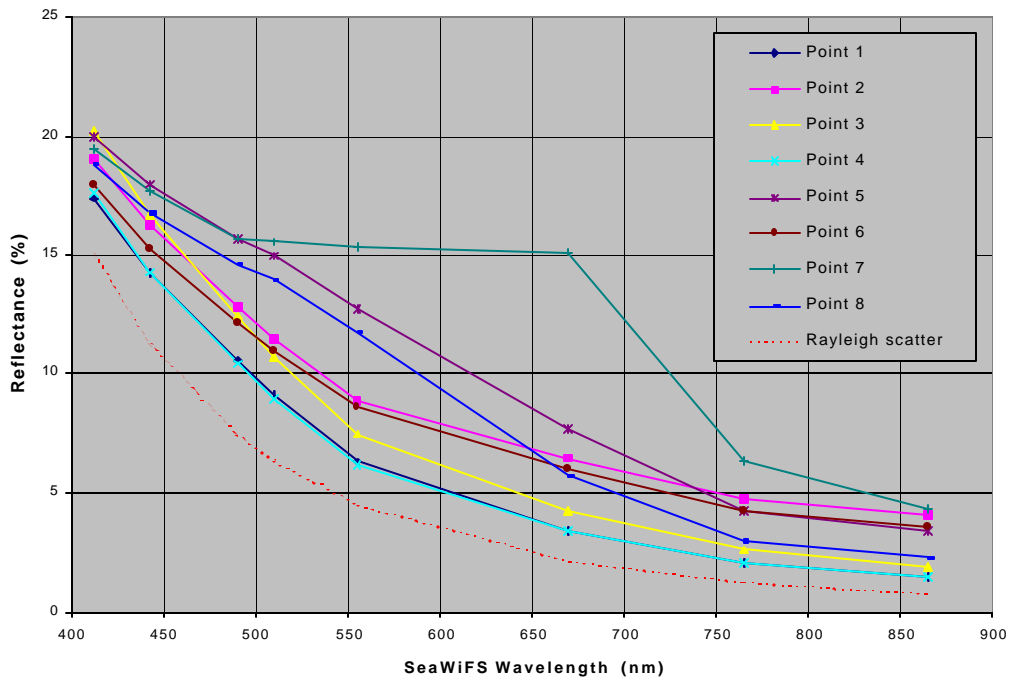


Figure 10. Reflectance spectra from April 15, 2001 for each location and Rayleigh scatter.

reflectance profile for an arbitrary initial reflectance value for channel one, 412 nm, of 15%. The reflective contribution from the water is greatest in the short wavelength, 400 to 500 nm region, and decreases to near zero by 670 nm.

The spectral profile for point 2, located over very low turbidity water and under a relatively heavy white haze with a slight red tint, shows a similar drop in reflectance as that of point 1. The significant difference is that all reflectance measurements are slightly higher than that of point one. It appears that the haze causes an increase of reflectance at all wavelengths nearly equally. The longer wavelength end of the profile, channels five thru eight, is elevated just barely greater than the short wavelength end of the spectrum, which explains the red tint. If all things were exactly equal at the water surface between the two points, which is difficult to determine and not guaranteed, then it would appear that the atmosphere over point 2 contains a particle size distribution that is weighted greater on the larger particle side. This seems to make sense, since the true color composite clearly shows a haze layer over point 2, and haze is caused by particles that are greater in size than air molecules.

The spectral profile for point 3, located over low turbidity water and under a light blue haze, also has a profile that closely resembles a Rayleigh scatter profile. In this case, the reflectance measurements are slightly elevated overall and more so at the short wavelength end of the spectrum. In this instance, many of the same remarks can be made as were made about point 2, the major difference being which end of the spectrum shows a biased elevation. In this case, the bias at the short wavelength end of the spectrum seems consistent with the true color composite that clearly shows a haze that is blue in color.

The spectral profile for point 4, located over very low turbidity water and under a very clear atmosphere, is nearly exactly the same as point 1. The arguments made for point one could be duplicated for this point.

The spectral profile for point 5, located over a region of medium turbidity water and under light haze with a red tint, is noticeably different than that of the points 1 thru 4. The profile here does not look like a Rayleigh scatter curve. The reflectance measurements drop almost linearly from channel one to channel six. When comparing

this profile against any of the preceding profiles, this difference in shape is readily apparent. Without in-situ water clarity and suspended sediment measurements, it is not possible to determine whether the increase in reflectance of the medium wavelength channels is due only to particles suspended in the water column or if it is a combination of both suspended particles and a chemical alteration of the waters actual color due to CDOM. By merely visual inspection of the true color composite image, it appears that the water of the area must contain a significant amount of suspended material.

The spectral profile for point 6, located over relatively low turbidity water and under a medium thick haze with a red tint, depicts a profile that is similar to points 1 thru 4 in that it closely represents a Rayleigh scatter profile. In this case, the long wavelength end of the spectrum has small but noticeably higher reflectance measurements, as compared to the first four points. This bias in the long wavelength end of the spectrum is consistent with a comparison of the true color image that shows that the haze has a red dominated tint. The reflectance measurements in the short wave end of the spectrum are relatively close to those of points 1 thru 4.

The spectral profile for point 7, located over the very high turbidity water of the Yangtze River outflow and under a very light haze, has the most unique characteristics of any over water point. The measured reflectance drops from channel one to three similar to that of the medium turbidity water of point 5. However, the profile becomes almost flat across from channel three to channel six. The reflectance measurements for channels three thru six are within 2 % of each other. The channel seven reflectance drops sharply to a value just slightly higher than the values measured for both medium turbidity water and clear water under high haze. The distinctive "hump" in this profile makes this point's profile very easy to isolate from the profiles of any of the other cases studied. This increased reflectance in channels three thru six, 490 nm to 670 nm respectively, is clearly evident in the true color composite. This region of highly turbid, sediment laden Yangtze River outflow moves out across the East China Sea in huge tan to muddy brown filaments and routinely covers an area over 100,000 square kilometers. As the sediment fan is dispersed to the southeast by the China Coastal Current and/or the Yellow Sea Coastal Current, the color slowly changes from muddy brown to green, and then eventually merging with the low turbidity blue sea. Like point 5, once past the obvious

muddy brown, sediment laden region, it is unclear what the dominant processes that are causing the green water color. Here, as well, it is quite possible that CDOM has altered the actual color of the water.

Point 8 is located over the extended Yangtze River outflow fan, further towards the center of the East China Sea, and is under a very light haze. The spectral profile for this point is very similar to that of point 5. The measured reflectance drops from channel one to channel six almost linearly, before flattening out at channels seven and eight. The reflectance values here, nearly equally across the entire spectrum, are just slightly lower than the corresponding reflectance values for point 5. It is unknown whether this drop is due to the particles being settled to a depth further in the water column or if the actual composition of the suspended particles is different, and thus causing the lower reflectance. It is worth noting that the profiles are nearly identical in shape, with point 8's reflectance just slightly lower.

The following discussion summarizes the analysis of the measured reflectance data for April 15. The eight locations can be reasonably separated into three groups using water turbidity as a discriminator. Points 1 thru 4 and 6 are located over low turbidity water. Points 5 and 8 are over medium turbidity and/or chemically altered water, and point 7 is over sediment laden, very high turbidity water.

The points located over clear, low turbidity water and under little or no haze display a profile that is very similar to a Rayleigh scatter profile. For those points located over clear water, but under haze of varying intensity and makeup, the profiles look similar to Rayleigh scatter profiles as well. However, in these cases, depending on the composition and size of the haze particles, the profile is elevated at one end of the spectrum or the other. The points located under smaller particle blue haze had profiles biased higher in the short wavelength end of the spectrum and the profiles for points located under larger particle tan or red tinted haze were biased in the long wavelength end of the spectrum.

The points located over medium turbidity water display a reflectance profile that decays nearly linearly from channel one to channel six. This profile can be clearly identified by this feature, when being compared to the low turbidity water cases. The

potential reason for this profile, partly stated earlier, may be due to the presence of a collection of particles that have a relatively evenly distributed physical size and/or an alteration of the actual water color, resulting from CDOM. Recall there are no in-situ measurements available for comparison.

Point 7, the only point located directly over the most highly turbid water of the region, displays a spectral reflectance profile that is the most unique of any of the locations studied. The tremendous amount of sediment being transported in to the East China Sea by the Yangtze River produces characteristics in the received reflectance profile that are unmistakable, when compared to other regional spectral profiles. This region of high turbidity water is a remarkable sight and stands out in any cloud free true color image. The greatly enhanced reflectance in the middle channels, caused by this sediment, is clearly evident in the April 15 image (Figure 9).

2. Case Study 2: April 13 2001 (SeaWiFS file 2001 103 041557)

Figure 11 is a true color composite image of the region with the same eight locations depicted. Figure 12 depicts the measured reflectance at the eight original locations as a function of wavelength. In the same manner as case one, the analysis was completed by comparing the characteristics of the spectral profiles to the true color composite. As before, each point will be discussed and the spectral characteristics identified.

The spectral profile for point 1, located over very clear water and under a light blue haze, is similar to a Rayleigh scatter curve, with slightly elevated reflectance values for channels one thru three. The increase in the reflectance in these channels is due to the haze that is present at this location. Since there is an increased reflectance in the shorter wavelengths, it is presumed that there is a disproportionately large amount of very small airborne particles.

The spectral profile for point 2, located over clear water and under a light blue haze, is nearly exactly the same as the profile for point one. The two are nearly indistinguishable. The analysis for this point is identical to point one. In case 1, this location was under a haze that had a red tint. In that instance, there were more large

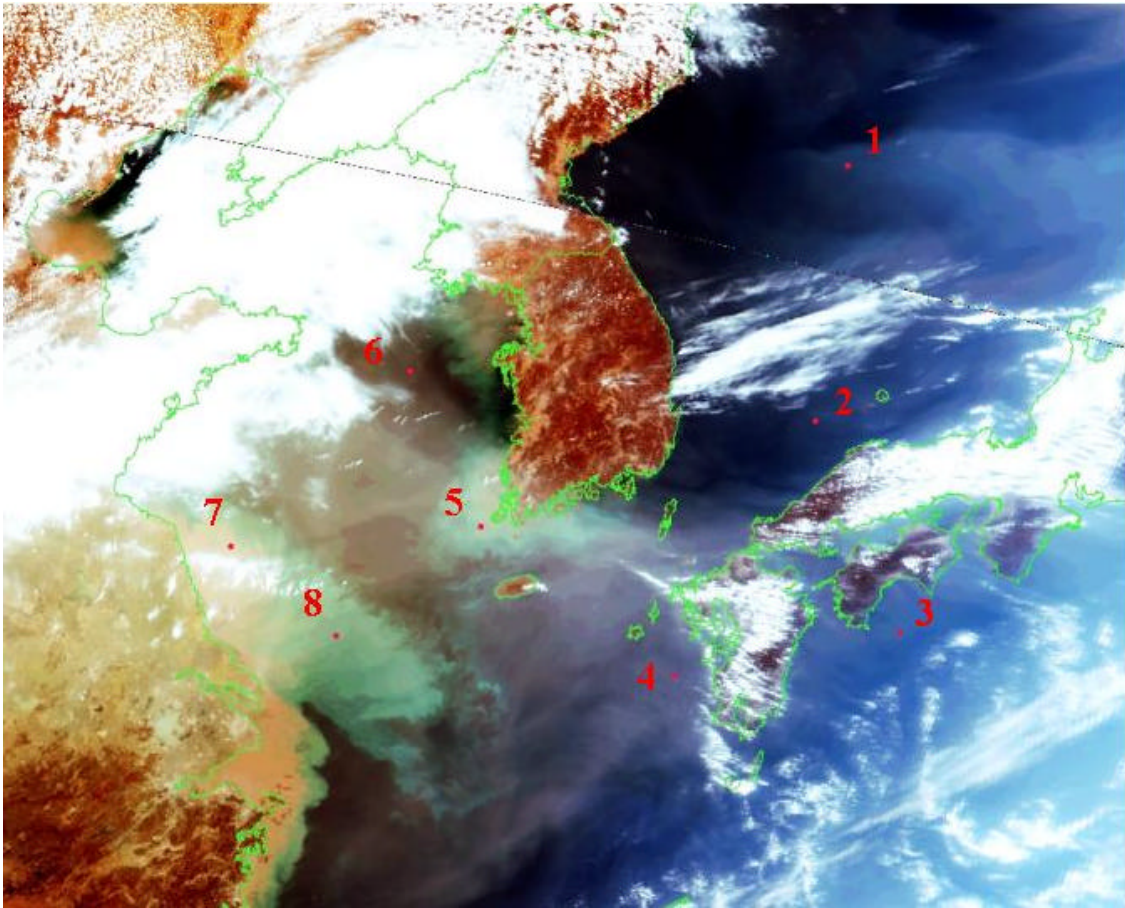


Figure 11. True color image from April 13, 2001, with the same eight study locations depicted.

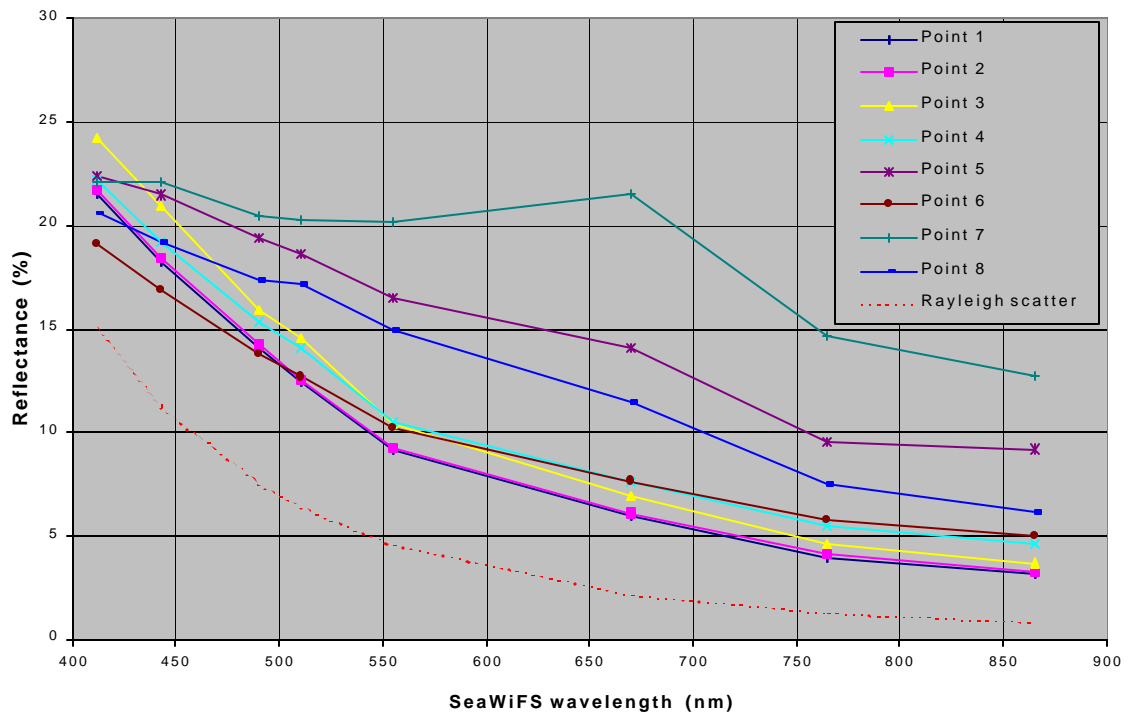


Figure 12. Reflectance spectra from April 13, 2001 for each location and Rayleigh scatter.

airborne particles to reflect the red wavelengths, which resulted in a spectrum that was slightly elevated at the long wavelength end.

The spectral profile for point 3, located over clear water and under a heavy blue haze, has the shape of a Rayleigh scatter curve, but is even more heavily biased in the blue wavelength end of the spectrum. The reflectance in the blue wavelengths for this point is as much as 3% higher than the corresponding channels for points 1 or 2. The profile rapidly begins to match the profiles of points 1 and 2, once past channel 4. The concentration of the very small airborne particles in this region must be greater than that of points 1 or 2 in order to cause this difference.

The spectral profile for point 4, located over dear water and under a heavy blue haze that is slightly tinted red, is similar to the other points described for this day, with the exception of the following. The reflectance is slightly higher in the red wavelength end of the spectrum. The reflectance at the blue wavelength end is not as great as that of the heavy blue haze of point 3. This indicates the presence of both very small particles, required for reflecting the blue wavelengths, and particles of larger size, which are reflecting the red wavelengths. This is the reason the haze has the red tint in the true color composite image.

Point 5 is located over medium turbidity water and under a heavy tan haze. Before describing the spectrum, it is worth noting that it is reasonable to expect that the measured reflectance spectrum will have traits that are a combination of both a turbid water signature and a heavy haze signature. The profile is similar to that of the same point in Case 1, April 15, in that the profile is nearly linear from channel one to channel six. However the medium to long wavelength reflectance is greater than that of Case 1, resulting in both a very slight hump at channel six and an overall higher reflectance in channels six thru eight. By examining the true color composite, it is possible to get the sense that the underlying turbidity signature is similar to Case 1, point 5, with the addition of an airborne haze that may contain some dust. If the haze does contain some percentage of dust, which scatters the longer wavelengths better, it would explain the characteristics of the profile.

The spectral profile for point 6, located over clear water and under a red haze, is very similar to a Rayleigh scatter curve. The essential difference can be seen in the elevated longer wavelength reflectance, due to large sized airborne particles.

The spectral profile for point 7, located in the highly turbid Yangtze River outflow region and under heavy tan haze, is significantly different from the other location profiles. As in Case 1, the profile has a disproportionately greater reflectance across channels four thru six. The channel six reflectance is high enough to cause the unique hump in the spectrum associated with water that is very high in suspended sediments. In addition to this feature, the reflectance of channels six, seven, and eight also appears to be increased (compared to case 1) by the airborne particles causing the haze.

Point 8 is located over the extended Yangtze River outflow fan and under a medium tan haze. The spectral profile is very similar to point 5, with the exception that the reflectance measurements, across the spectrum, are just slightly lower. As stated in case 1, it is difficult to determine whether the received reflectance measurements are due to settling of the suspended particles lower in the water column, or if it is a result of CDOM changing the water color.

The following discussion summarizes the analysis of the measured reflectance data for April 13. Recall, points 1 thru 4 and 6 are located over low turbidity water, points 5 and 8 are over medium turbidity and/or chemically altered water, and point 7 is over sediment laden, very high turbidity water.

Similar to Case 1, the points located over clear, low turbidity water and under little or no haze display a profile that is very similar to a Rayleigh scatter profile. For those points located over clear water, but under haze of varying intensity and makeup, the profiles look similar to Rayleigh scatter profiles as well. However, in these cases, depending on the composition and size of the haze particles, the profile is elevated at one end of the spectrum or the other. The points located under smaller particle blue haze had profiles biased higher in the short wavelength end of the spectrum and the profiles for points located under larger particle tan or red tinted haze were biased in the long wavelength end of the spectrum.

As in Case 1, the points located over medium turbidity water display a reflectance profile that decays nearly linearly from channel one to channel six. This profile can be clearly identified by this feature, when being compared to the low turbidity water cases. The potential reason for this profile, as stated earlier, may be due to the presence of a collection of particles that have a relatively evenly distributed physical size, due to the larger particles settling lower in the water column and/or a chemical alteration of the actual water color, resulting from CDOM.

Point 7 has a spectral reflectance profile that is, once again, the most unique of any location studied. Both the sediment causing the greatly enhanced reflectance in the middle channels, and the tan haze causing the increased reflectance in the longer wavelength channels, are clearly evident in the true color composite image (Figure 11).

3. Case Study 3: April 10, 2001 (SeaWiFS file 2001 100 034527)

This case study is slightly different than the previous two. After performing an analysis in the same manner as Case Studies 1 and 2, for a total of eight individual days of data, it was determined that a closer investigation of the spectral reflectance profiles for thick airborne dust and clouds was necessary. The data from April 10 provided the best opportunity for this comparison. In this case, the region of interest is the Japan Sea and it contains a massive airborne dust plume and numerous clouds. Figure 13 is a true color composite of the area and Figure 14 shows the reflectance profiles for the locations examined. Four locations were chosen for evaluation, two within the dust plume (pts 3 and 4), one within a cloud over the dust plume (pt 2), and one within a cloud not associated with the dust plume (pt 1). The reflectance profiles here are considerably different than the profiles of Cases 1 and 2. In the preceding cases, the measured reflectance spectrum may have been influenced by atmospheric aerosols, but were still primarily providing information of surface properties. In this case, the atmospheric event is completely masking the surface and thus the reflectance information is entirely from the atmospheric constituents, specifically cloud or dust.

Point 1 is located in a cloud of medium thickness, over very clear water, just off shore of the northernmost part of North Korea. This reflectance profile did not appear as

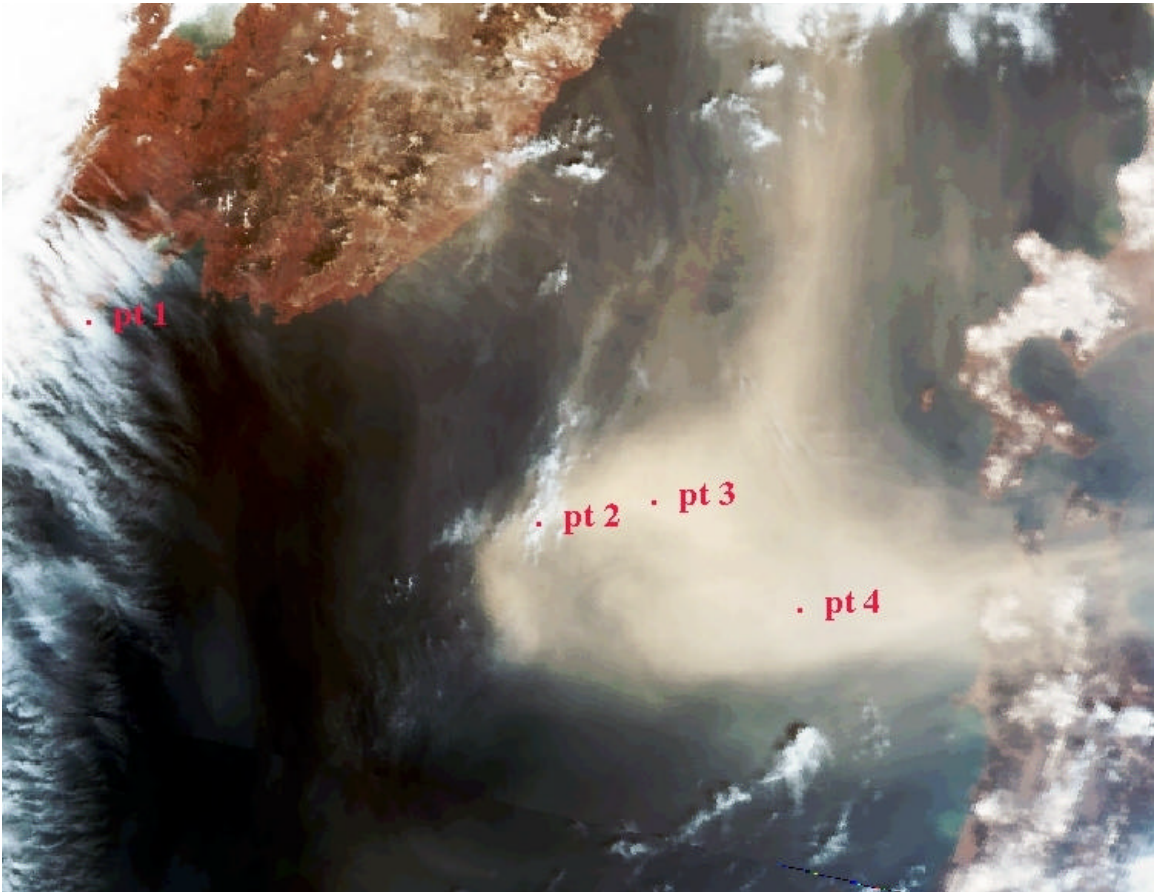


Figure 13. True color image from April 10, 2001, with study locations depicted.

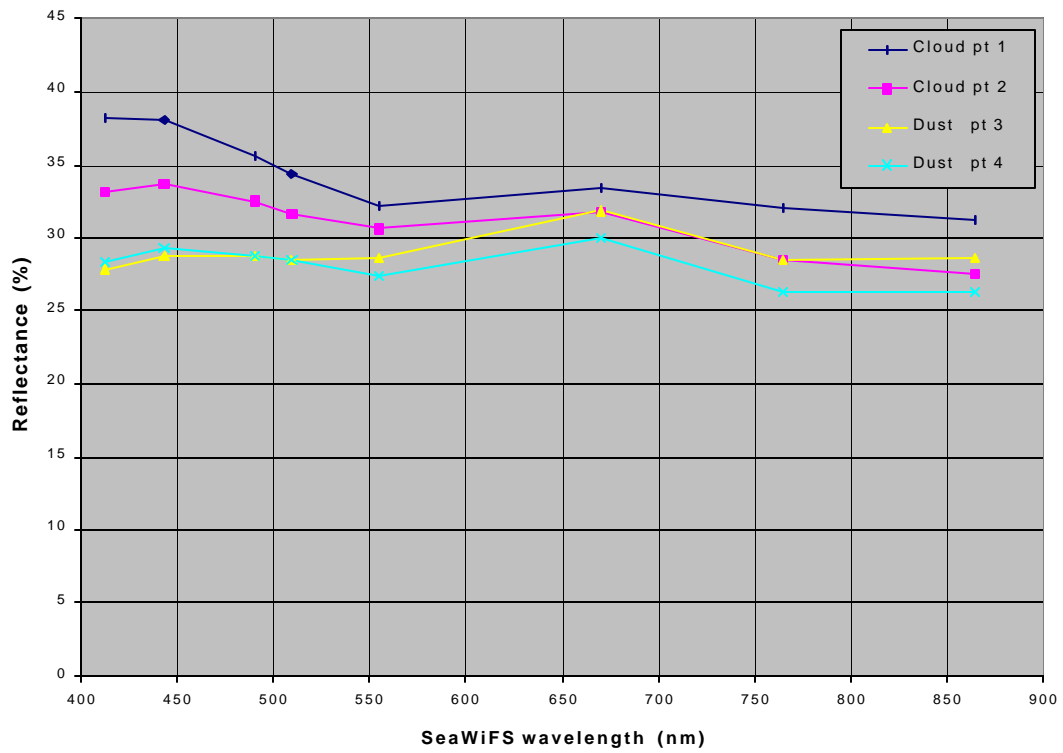


Figure 14. Reflectance spectra from April 10, 2001 for clouds and dust.

expected. Prior to producing the plot, it was expected that the reflectance would be essentially equal across all wavelengths, because it is assumed that clouds scatter all visible wavelengths equally. This, however, was not the case. The profile has some features that appear to be wavelength dependent. It is possible that the cloud is made up of both water droplets and ice crystals. This would alter its reflectance properties. Though the profile does have some form that looks as though it may be of use for future discrimination algorithms, it must be noted that the values are all very close to one another, ranging from 38% for channel one to 32% for channel eight. The most valuable characteristic of this profile is the decrease in reflectance from the blue wavelengths to the red wavelengths.

Point 2, located in a cloud of medium thickness and apparently above the dust plume, has a spectral profile that is very similar to the profile for point 1. The most notable difference between the two profiles is the overall lower reflectance of point 2. Secondly, point 2 shows a slight increase in reflectance between channels one and two. As was the case for point 1, it must be noted that the reflectance values are across the spectrum are all within 6% of each other. This difference in reflectance is almost the same as the overall difference between points 1 and 2 for most of the spectrum. As with point 1, the difference in reflectance between neighboring channels is not as significant as the overall decrease in reflectance from the blue wavelengths to the red wavelengths.

Point 3, located in an optically thick region of the northern part of the dust plume, has a spectral reflectance profile that is different from the cloud points. Here the reflectance is more even across the spectrum. Channel six is the noticeably elevated channel. This is caused by the large sized dust particles, which reflect the red wavelengths more. The difference in reflectance across the spectrum is less than 5% and is less than that of the cloud points. The significant difference between this point and the cloud points is that there is very little decrease in reflectance from the blue wavelength end of the spectrum the red wavelength end. In fact, the channel eight reflectance is larger than the channel two reflectance. This was never the case in any cloud reflectance examinations.

Point 4, located in an optically thick part of the southern portion of the dust plume, is extremely similar to the profile for point 3. The difference is that the longer wavelength end of the spectrum has slightly less reflectance than that of point 3. The cause of this lower reflectance in the 555 to 865 nm range is presumably due to the difference in the size distribution of the airborne particles. In this case, it is expected there are fewer large particles to preferentially scatter the longer wavelengths. As was the case for point 3, the difference in reflectance from the short wavelength end of the spectrum to the long wavelength end is very small. Here again, the reflectance difference across the entire spectrum is less than 5%.

In order to summarize the information obtained from this case study, the cloud points will be grouped together and discussed first and then compared to the two dust points. With the exception of the overall decreasing trend from short wavelength to long wavelength, the variation of the cloud profiles are too small to be of any value for algorithm use. It is interesting that the cloud profiles resulted in a spectrum that was less flat than dust, even though it was expected that the clouds would reflect all wavelengths equally. It is possible that the clouds were made up of both water droplets and ice crystals, which causes changes in the reflectance. These changes are beyond the scope of this study. Although the actual cause for the occurrence is still unknown, this overall decrease in reflectance across the spectrum will be significant for algorithm development, as will be discussed in following sections.

The spectrum revealed for the dust locations was surprisingly flatter than those of the clouds. The most significant feature of the dust locations is that the overall decrease from the short wavelength end of the spectrum to the long wavelength end is very low or actually negative. This will aid in algorithm development, as will be discussed in the following sections.

4. Regional Background Reflectance

Determining the best method to define regional background reflectance was a challenging problem. The motivation to achieve this was to obtain better baseline ocean reflectance values for input into the current SeaWiFS aerosol optical depth algorithm.

During the course of the individual spectral examinations, it became apparent that the reflectance at channel six was the most affected by the airborne atmospheric constituents. It was determined that the best way to obtain the baseline background reflectance was to compose a composite measurement data set, using channel six as the focus of the discrimination process. By minimizing channel six, it is possible to eliminate the maximum amount of atmospheric contribution. A pixel-by-pixel analysis was completed for the entire region, and the dataset that contained the pixel with the lowest channel six reflectance was used to obtain the reflectance values for all eight channels.

The process to create these data sets, one for each of the eight channels, started by running a cloud mask on all of the data. The cloud mask program uses thresholds to determine cutoffs for discriminating what is or is not clouds. Those values over the threshold are not considered in the calculations that follow this step. Following the cloud masking process, the computer program would perform a pixel-by-pixel evaluation. For each pixel, the daily data set that contained the lowest reflectance measurement for channel six was determined and then the values from that day's data was stored for all of the eight channels. The result of this filtering program is a data set containing reflectance measurements for all eight channels, from the day where the channel six reflectance was lowest for the time period. Figure 15 is a single channel image result for channel six. Figure 16 is a true color composite made from this created data set, using channels two, four, and six for blue, green and red, respectively. Using the information contained in these data sets, follow-on work may be initiated to isolate specific regions of similar reflectance. This regional reflectance value could then be used as an input parameter in the aerosol optical depth program.

This composite process produced a true color image that provided information regarding the optical properties of both the atmosphere and ocean surface. By closely examining Figure 16, it can be seen that large areas of both the East China Sea and the Sea of Japan still appear to be covered with haze of differing intensities. This is a result of having a limited number of data sets for the composite process. These hazy regions are still evident because there was no data set during the study period that did not contain some degree of haze. The bluish regions are regions that still contain some atmospheric contribution. The greenish regions are more representative of the true ocean color under

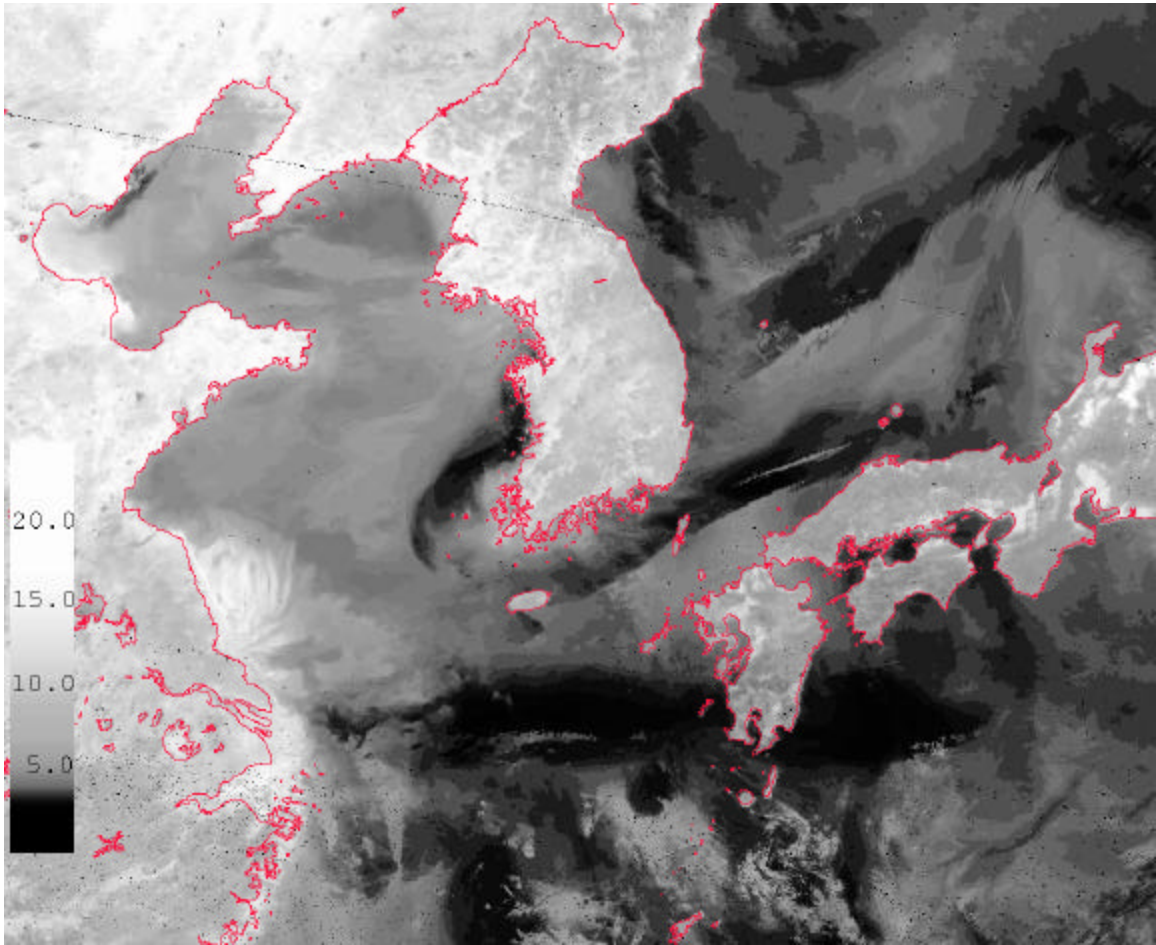


Figure 15. Minimum channel six reflectance (%) at each pixel for entire study period.

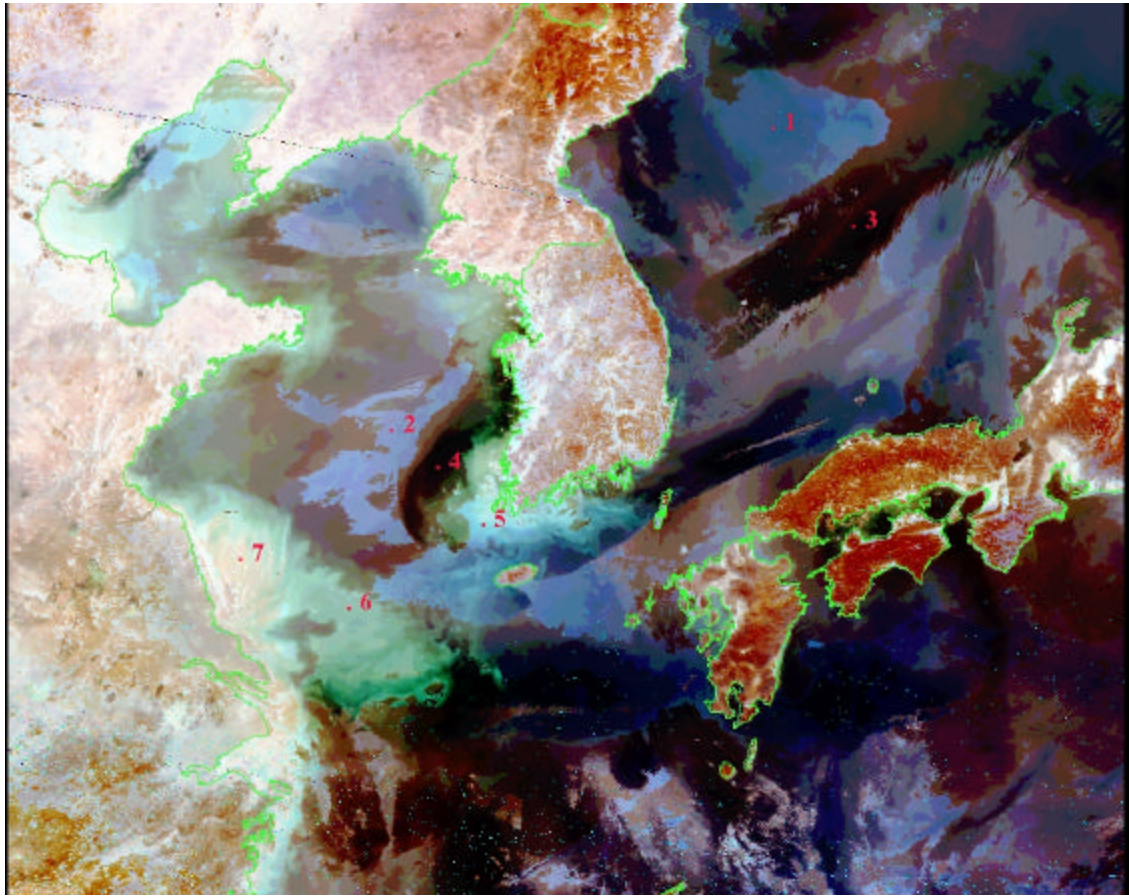


Figure 16. Color composite using channels two, four and six for red, green and blue, respectively, from channel six minimization process. Also depicted are the seven study locations.

a clear atmosphere. Another point of interest is the hammer like feature in the Yangtze River outflow fan. This is presumably caused by an unusually deep intrusion of the Taiwan Warm Current into the East China Sea. This is a somewhat anomalous situation and the data set containing this feature could be omitted from the regional background data set, if it was determined that this occurs rarely enough to accurately generalize the features of the area without it. A much longer data set would be required to determine whether or not this is reasonable. Additionally, this work merely demonstrates the capability to produce a meaningful data set that could be used to improve the operational programs. In order to characterize the background reflectance truly accurately, a much longer data set would be required to expose the seasonal and annual variability of the regional reflectance.

In order to try to quantify the results of this composite process, seven locations were chosen and the associated reflectance for each channel was determined. Figure 16 is the color composite showing the seven study locations. Figure 17 shows the reflectance profiles of these seven locations. By examining these profiles it is possible to determine the magnitude of the background reflectance at each of the different wavelengths. Using statistical composite techniques, it would be possible to obtain seasonal or annual regional reflectance estimates for the differing oceanic regions. Those results could then be used as input parameters in the aerosol optical depth programs to account for the higher reflectance that some regions routinely experience. Further work in this area was beyond the scope of this study, but should certainly be the focus of future studies.

5. Experimental Algorithms

During the initial analysis, many points were examined and their spectral characteristics identified. In this section, the process used to determine potentially useful algorithms is discussed. In order to more easily compare regions of drastically different spectral characteristics, a plot of the spectral profiles of five locations from April 15 is presented in Figure 18. These points represent regions with the following environmental conditions: 1) clear air over low turbidity water, 2) blue haze over low turbidity water, 3)

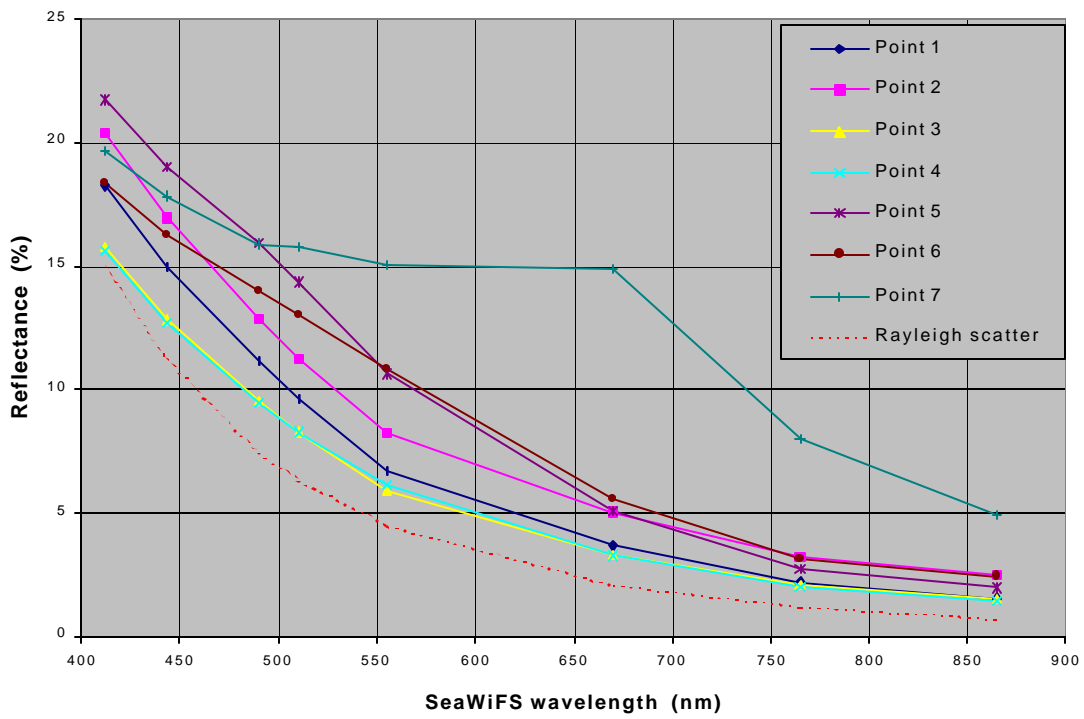


Figure 17. Reflectance spectra for channel six composite process.

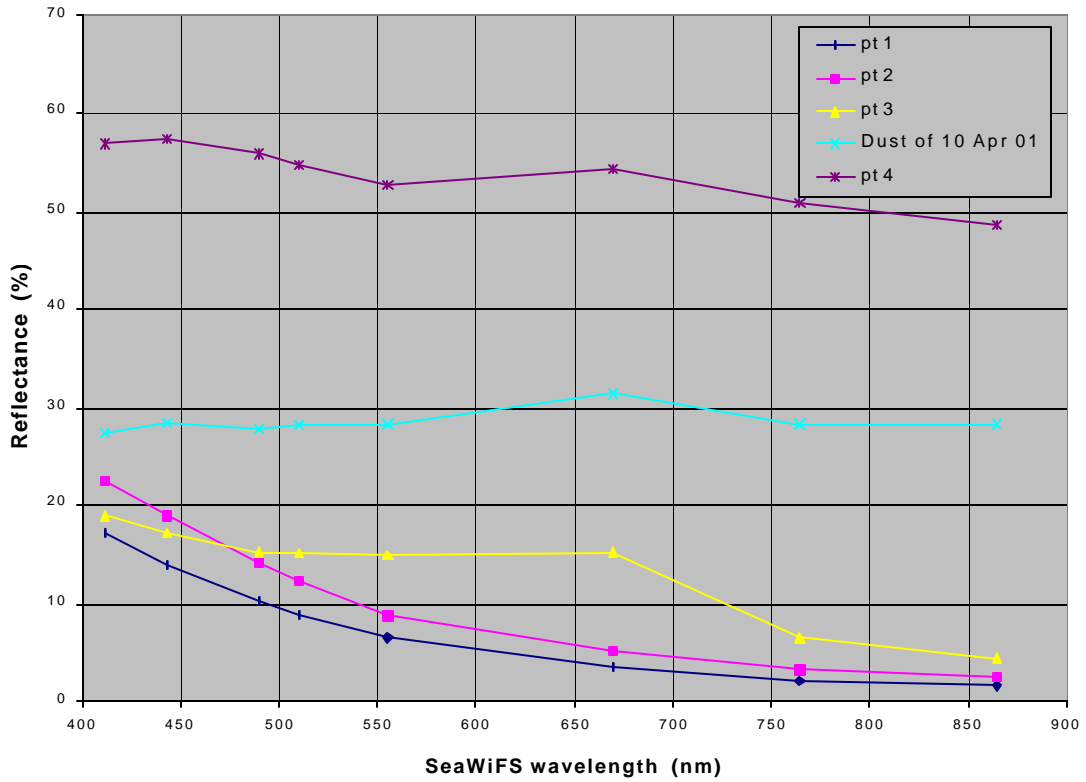


Figure 18. Reflectance spectra of four study locations from April 15 and one location from April 10 (dust).

clear air over high turbidity water, 4) cloud, and 5) a profile from the center of the dust storm of April 10. Figure 19 is a true color composite image depicting the exact locations of the analysis, with the exception of the April 10 dust point.

Many noteworthy differences in the spectral profiles presented can be identified. In lieu of specifying each and every one, only the features used to create the proposed algorithm will be discussed. The first and most successful algorithm was created to identify areas of airborne dust. The second algorithm was created to identify regions of high ocean turbidity.

a. Airborne Dust Identifier

The algorithm can be used to identify the geographic distribution and qualitative intensity of airborne dust in the atmosphere. The algorithm performs three individual calculations on each pixel in the scene. First, the channel two reflectance is examined and all values over 30% are omitted. This process eliminates nearly all areas of cloud, with the exception of the thin cloud edges - the most difficult problem faced in any cloud masking attempt. None of the cases of airborne dust revealed reflectance in channel two above 30%, therefore the dust would not be masked. Second, the channel eight reflectance is examined and all values below 20% are omitted. This eliminates all surface contributions. It is possible for thin dust to be masked by this process. This is an inherent problem with any program that uses thresholds and one that is unavoidable. The final step in the process is to divide the channel eight reflectance by the channel two reflectance. This produces a data set that contains values that are large where the channel eight to channel two reflectance ratio is large. This process essentially "looks" for a spectrum that is flat or increasing from channel two to channel eight, which is characteristic of a dust spectrum. Recall, a spectrum for cloud would decrease from channel two to channel eight. The higher the value the more likely the pixel is experiencing dust. Figure 20 is an image that depicts the regional dust extent and intensity for April 10. Figure 21 is a true color composite of the same area. Figure 22 is an image created using the airborne dust identifier algorithm on the data from April 15, and Figure 23 is the true color image of the April 15. On April 15, there was no concentrated airborne dust present. The algorithm seems to produce very good results

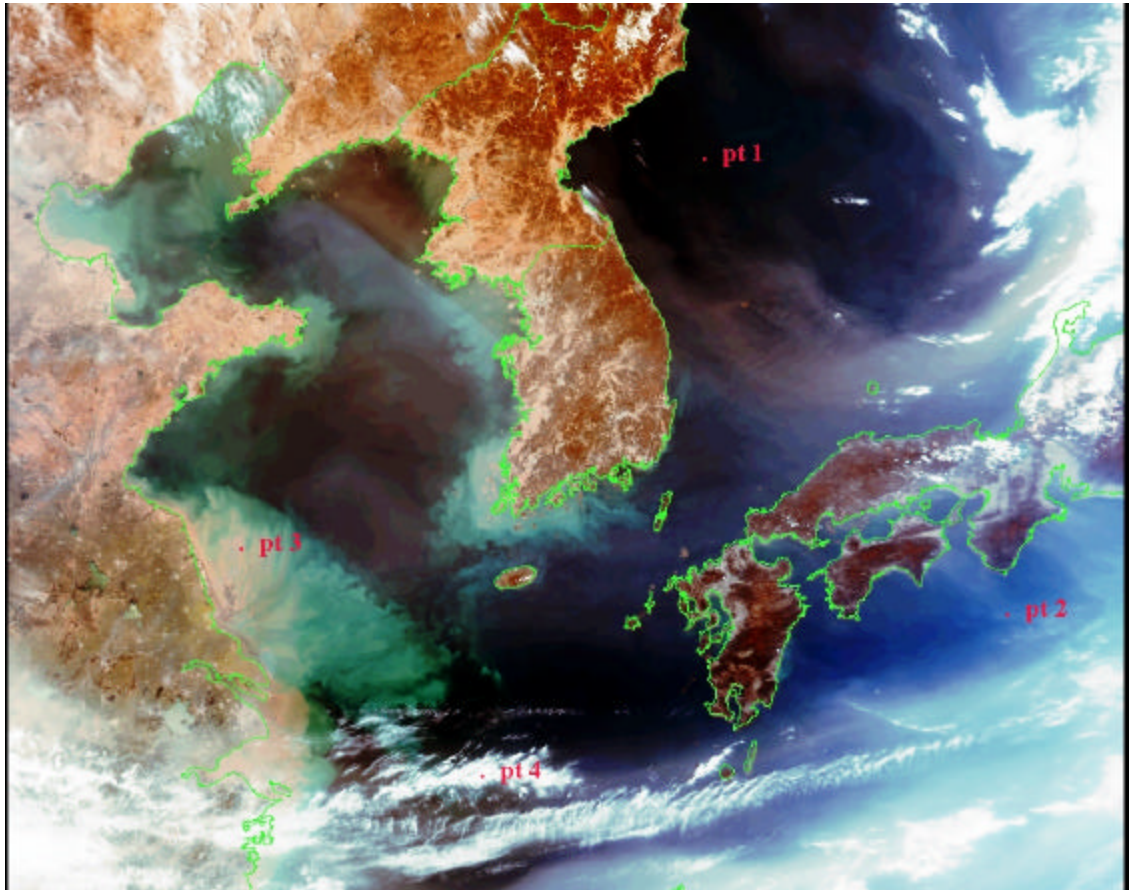


Figure 19. True color image from April 15, with four study locations depicted.

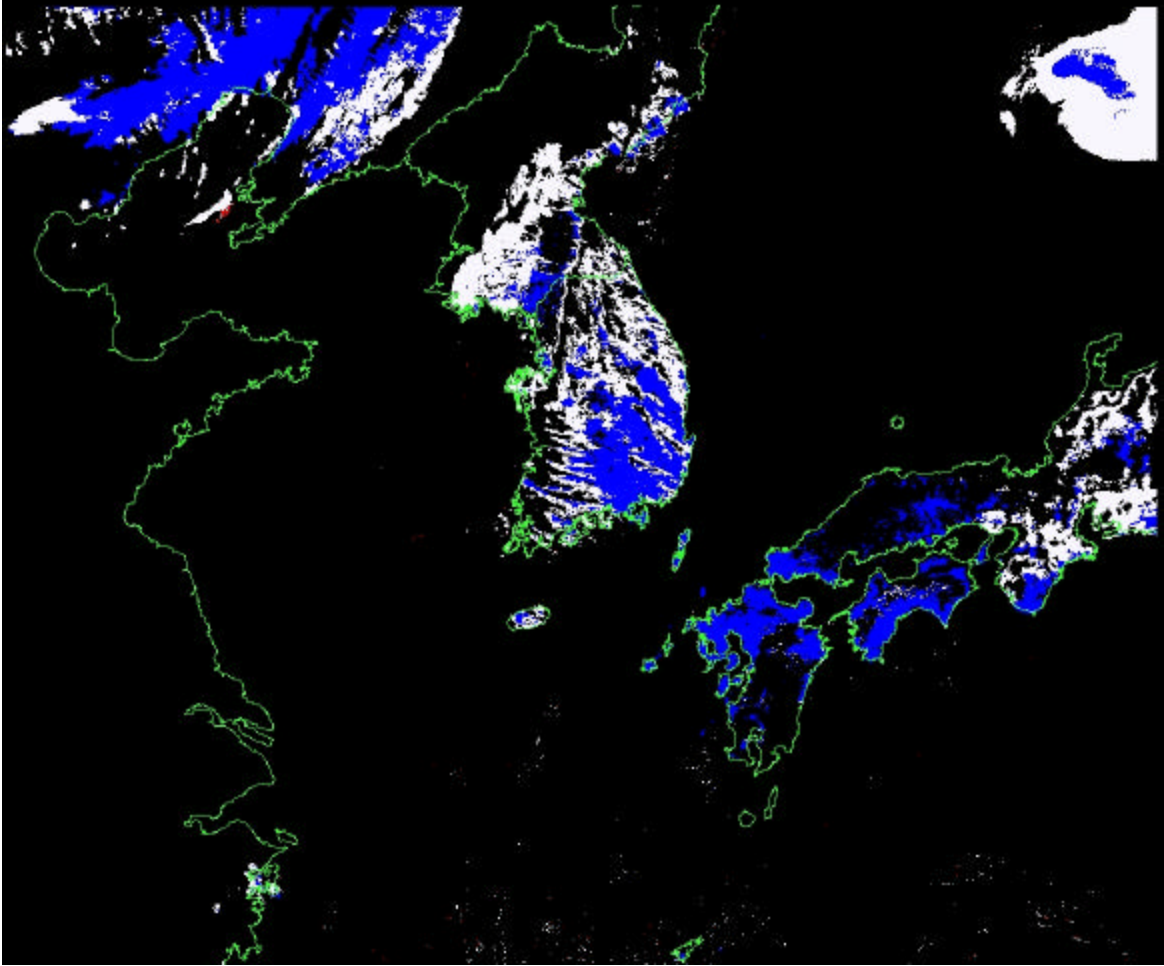


Figure 20. Image created from the dust identification algorithm for April 10.

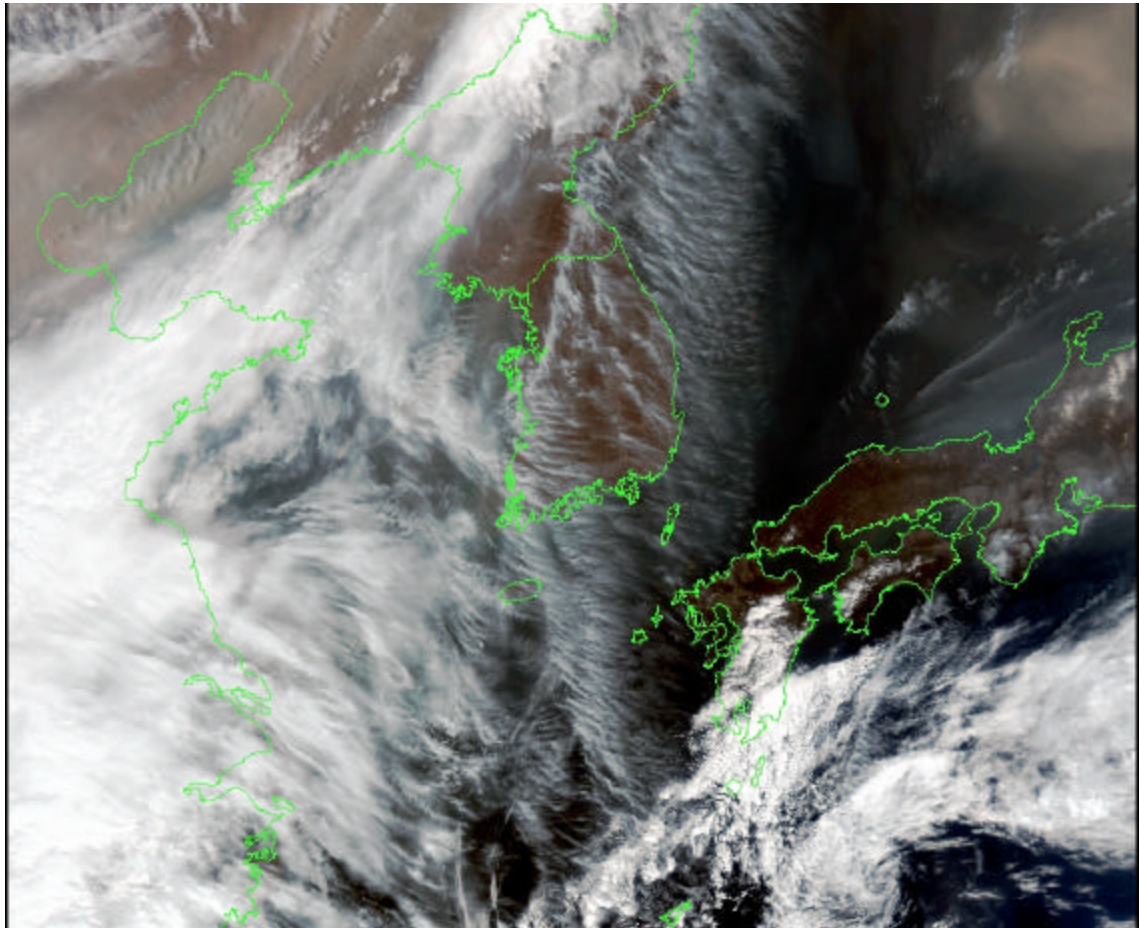


Figure 21. True color image from April 10, showing dust storm in upper right corner.

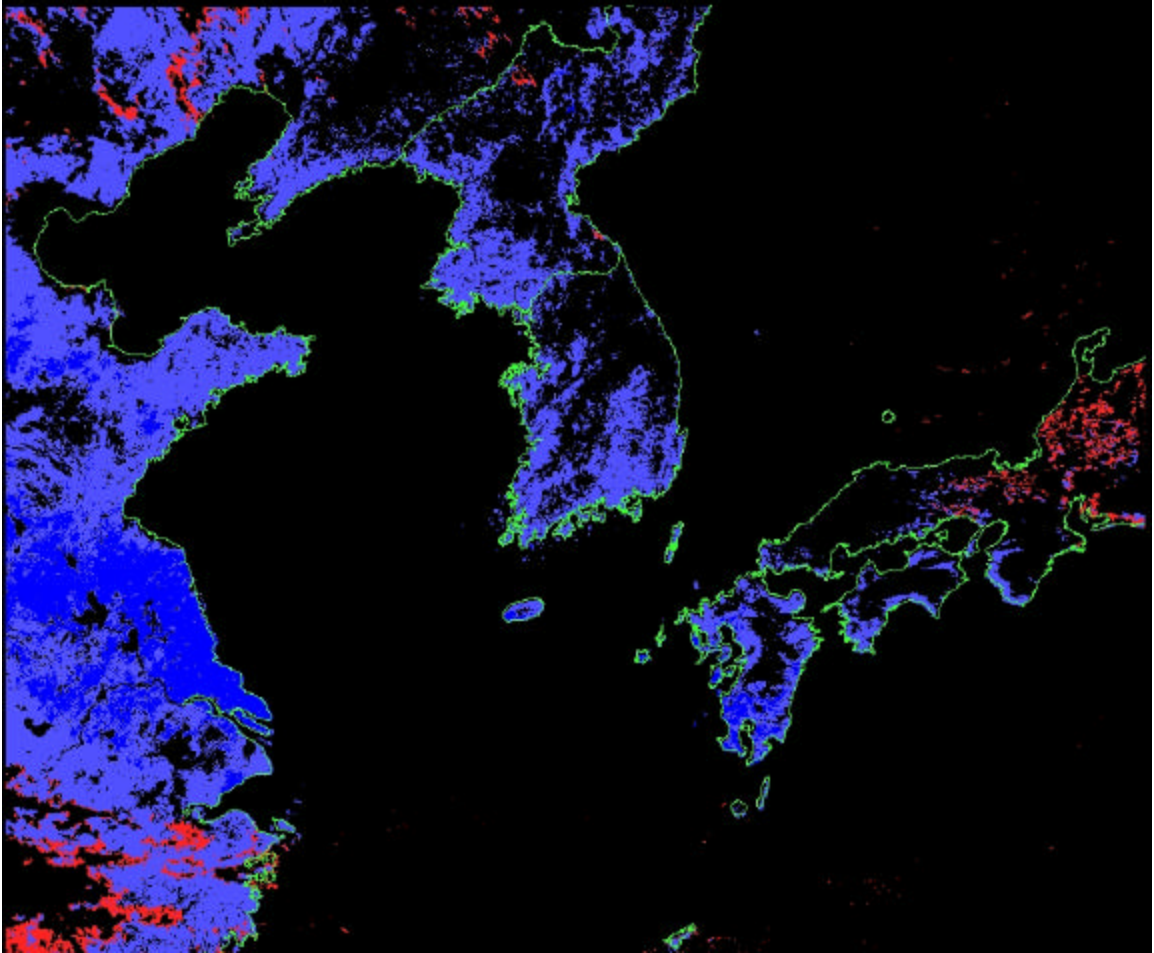


Figure 22. Image created from the dust identification algorithm for April 15.

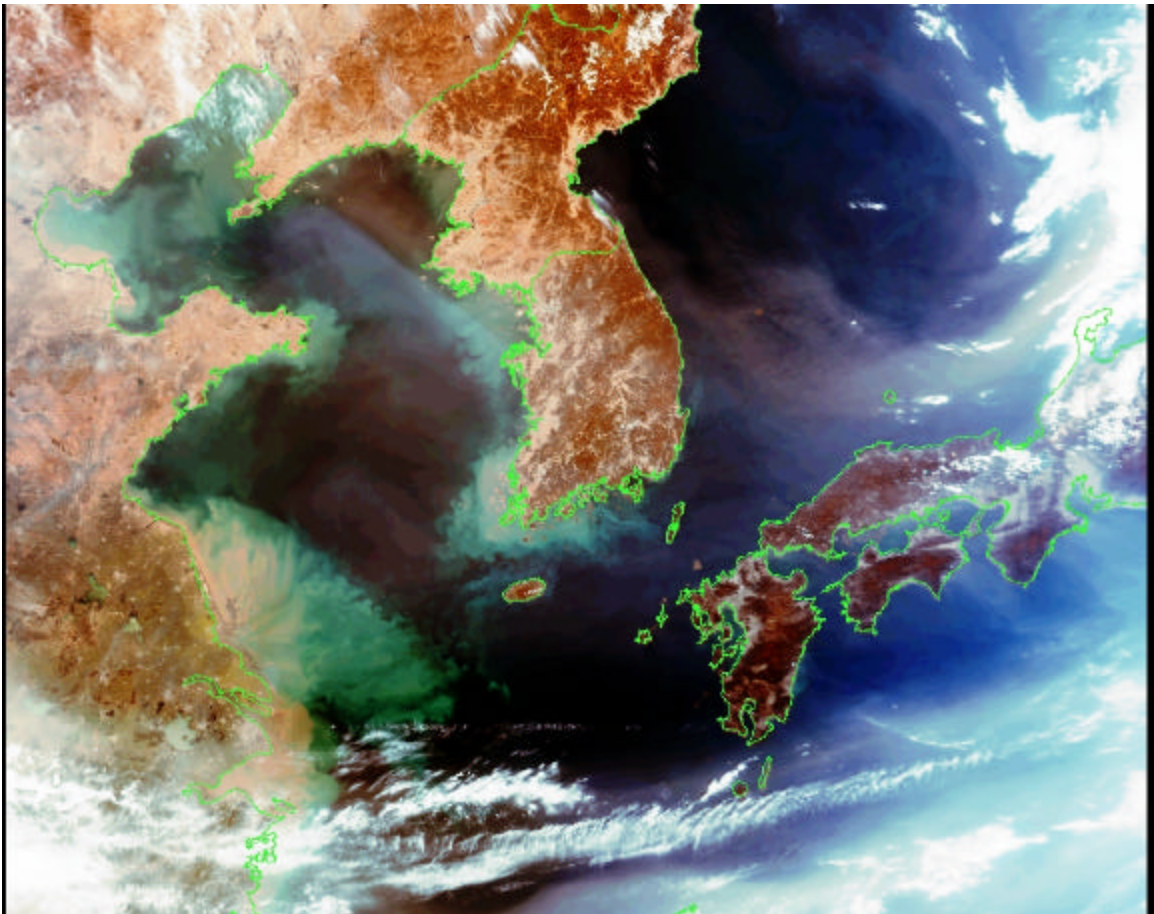


Figure 23. True color image from April 15.

and nearly zero false indications in the April 15 image. This can be seen if one compares the results of the two cases.

i. Oceanic Turbidity Identifier

In a similar fashion to the dust identification algorithm, the turbidity identification algorithm attempts to identify the geographic distribution and qualitative intensity of the ocean turbidity in the region. The principle of this algorithm is to exploit the large drop in reflectance between channels six and seven and the very small drop in reflectance between channels four and five that appear in the profiles of high turbidity water. Refer to figure 18 for the profiles of various environmental features from April 15. This algorithm executes a four-calculation process to produce the final data set. Initially, channel six reflectance is screened to eliminate all pixel values below 3.7%. This masks the very low turbidity water. The algorithm then calculates the ratio of channel six divided by channel seven and another of channel four divided by five. For high turbidity water, the values would be large for the first ratio and small for the second ratio. The final step in the calculation is to divide the ratio of channels six and seven by the ratio of channels four and five. Once all calculations have been completed, each pixel will have a value whose size is determined by the intensity of the oceanic turbidity. Figure 23 is a true color image of April 15 and Figure 24 is the algorithm calculated image of the regional turbidity. A second day's data was evaluated with the same process. Figures 25 and 26 are the true color image and the algorithm calculated regional turbidity for April 13. This process appears to work well. In the future, it may be possible to determine quantitative intensities by coupling this information with in-situ data. This should be the subject of future studies.

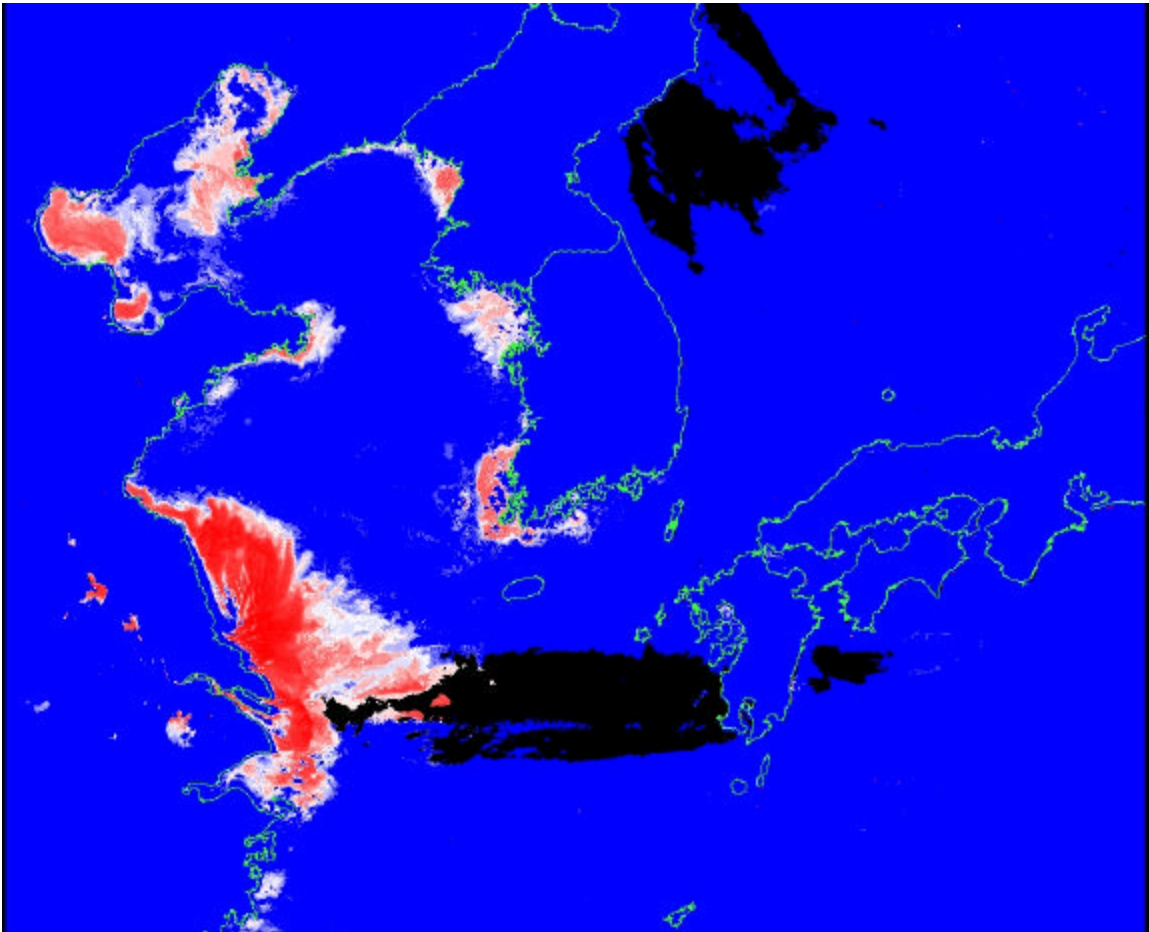


Figure 24. Image created from the turbidity identification algorithm for April 15.

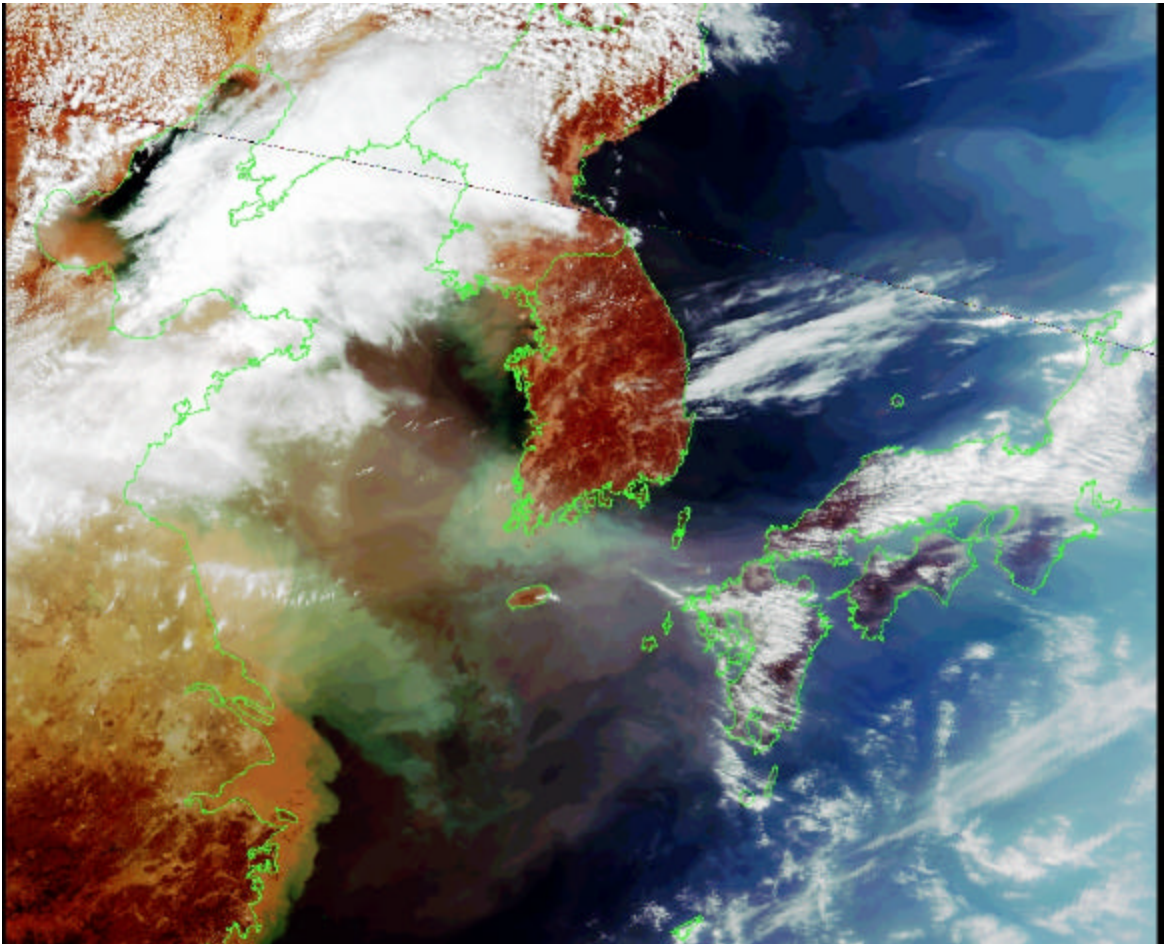


Figure 25. True color image from April 13.

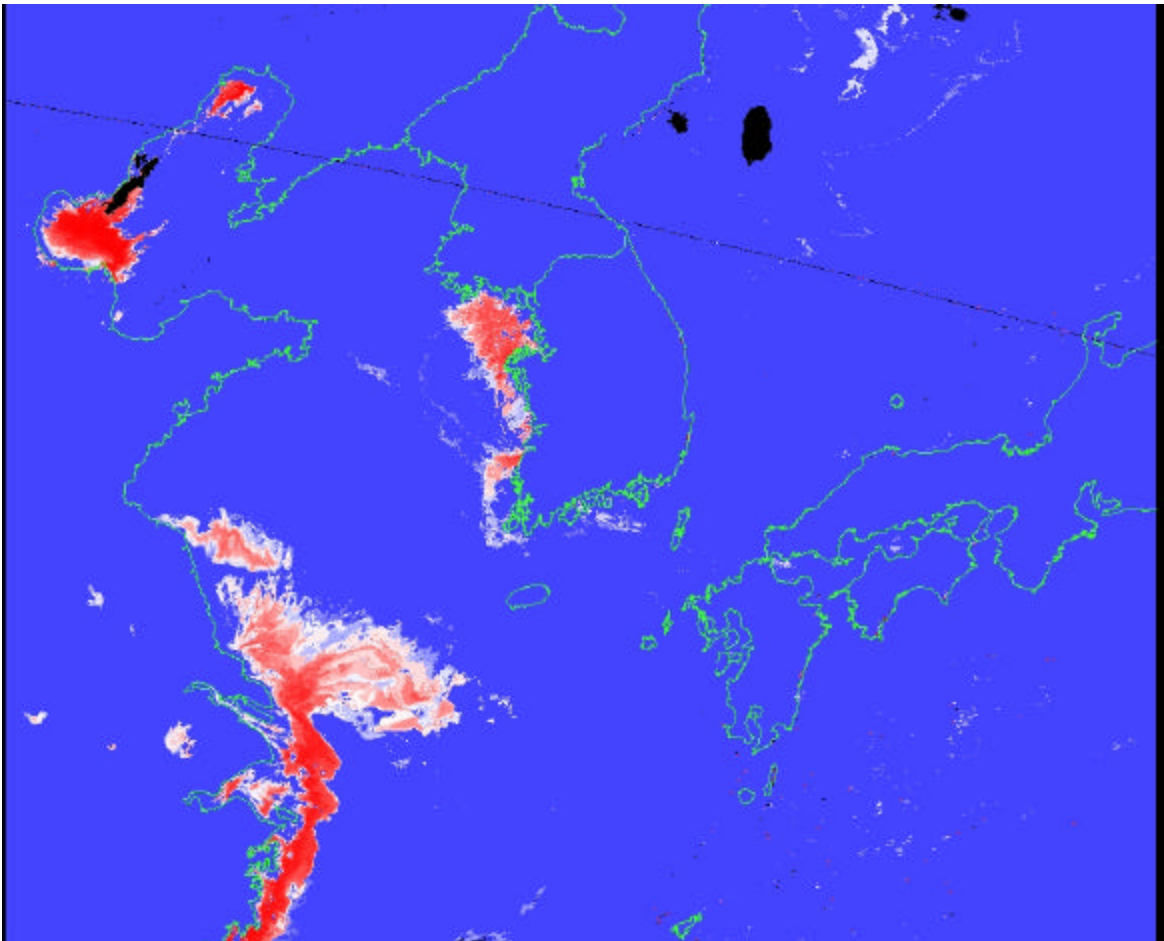


Figure 26. Image created from the turbidity identification algorithm for April 13.

THIS PAGE INTENTIONALLY LEFT BLANK

VI. CONCLUSIONS AND RECOMMENDATIONS

A. CONCLUSIONS

Using Visible wavelength reflectance data obtained by the Sea-viewing Wide Field-of-view Sensor (SeaWiFS), during the Asian Region Aerosol Characterization Experiment (ACE-Asia), an in-depth area study was completed focusing on the reflective properties of the atmosphere and ocean in the Japan and East China Sea region. Airborne dust and highly turbid water are dominant features in the region and are present on a daily basis. The primary goals of this study were to accurately determine the unique spectral signatures of these atmospheric and oceanic features, determine regional background reflectance values for possible inclusion in the next generation of aerosol optical depth programs, and develop algorithms capable of identifying regions experiencing high concentrations of airborne dust or high ocean turbidity. Because many operational systems rely on sending and receiving visible wavelength energy, it is important to investigate the effects environmental factors have on the transmission, absorption and scattering of this energy. This study will aid in the development of new and improved products to more accurately describe the theater of operations, which in turn will enable future military planners and on scene commanders to increase their situational awareness of the operational environment.

The first of these goals was accomplished by examining the spectral profiles of eight regional locations for each cloud free SeaWiFS overpass available. At each location, the reflectance of each SeaWiFS channel was determined and a spectral profile created. By examining the resulting spectra, it was possible to identify characteristic features of the profile that were unique to the specific atmospheric and/or oceanic state present at the time. Once this process had been completed for all overpasses, a set of general spectral signatures was established that were representative of the different atmospheric and oceanic states. The primary environmental signatures describe the following conditions: clear air over low turbidity water, clear air over high turbidity water, blue haze over low turbidity water, brown or red haze over low turbidity water, airborne dust over low or high turbidity water and clouds.

The second goal of the study was to determine the regional oceanic background reflectance. This is important because the current aerosol optical depth programs typically consider the ocean background to have a zero or near zero reflectance. In the East China Sea region, this is certainly not the case. The high sediment loading caused by the Yellow and Yangtze River discharge has great reflective properties across the visible spectrum. After examining numerous spectral profiles for varying air/ocean states, examining how differing atmospheric and oceanic properties effected the signatures, it was determined that the measured reflectance of channel six (670 nm) was most affected by atmospheric contaminants. Focusing on this channel six response to atmospheric contaminants, a method of determining the background reflectance was developed. A composite data set was created by isolating the lowest channel six reflectance measurement for each pixel from the entire series of overpasses. Once the lowest channel six reflectance value was determined, that value along with the reflectance for the other seven channels was stored. By using the results of this process, it was possible to create a color composite from channels two, four and six (blue, green and red, respectively) that exposed the ocean regions routinely experiencing high turbidity. Additionally, from this data set quantitative reflectance values can be estimated for specific oceanic areas within the region. These values can then be entered into the aerosol optical depth programs to improve their performance. A very long dataset would be required to produce a comprehensive product correctly representing the seasonal and annual variability in the regional oceanic reflectance.

The last goal of the study was to create algorithms to identify airborne dust over the ocean and high ocean turbidity. The algorithms were designed by examining the general spectral profiles of varying atmospheric and oceanic states and exploiting their unique characteristics. The algorithm created to identify airborne dust exploits the typically small decrease in reflectance from channel two (443 nm) to channel eight (865 nm). This feature appears to be unique to airborne dust. This algorithm will identify the geographic extent and a qualitative intensity of the airborne dust. Successful test cases were completed for regional dust events and correlate well when compared with true

color images. A turbidity identifier was developed using a similar technique. As in the dust case, the unique characteristics of the spectral profile of highly turbid water was determined and exploited. These characteristics were the typically large drop in reflectance between channels six (670 nm) and seven (765 nm) and the small or non-existent drop from channel four (510 nm) to five (555 nm). This algorithm produced adequate results but did have some limitations. Like the dust identifier, this algorithm will depict the geographic extent and a qualitative intensity of the turbidity.

B. RECOMMENDATIONS

The results contained in this study provide evidence that spaceborne sensors capable of measuring discrete visible wavelength radiation will allow scientists and researchers to greatly enhance our understanding of the environment in which we live and are required to execute military operations. The capability to discriminate even finer detail in spectral signatures will increase with the advent of multispectral and hyperspectral sensors. This will allow scientist and researchers to perform even more in-depth study of these processes. Suggestions for further studies include the following: 1) collection of a much longer data set, in order to more accurately determine the background reflectance and its seasonal or annual variability, 2) incorporation of the regional background reflectance into the current aerosol optical depth programs to improve their performance, 3) investigating comparisons between in situ measured intensities of airborne dust and ocean turbidity and the intensities derived by the airborne dust or ocean turbidity algorithms, 4) expanded research on the variations in the reflected visible light returned from clouds of varying types for possible development of cloud classification processes.

THIS PAGE INTENTIONALLY LEFT BLANK

LIST OF REFERENCES

- 1) <http://seawifs.gsfc.nasa.gov/SEAWIFS/SEASTAR/SPACECRAFT.html>
- 2) Clark, D.K., 1981: Phytoplankton pigment algorithms for the Nimbus-7 CZCS. *Oceanography from Space*, J.F.R. Gower, Ed., Plenum Press, 227-237.
- 3) Wehrli, C. "Extraterrestrial Solar Spectrum", Publication no. 615, Physikalisch-Meteorologisches Observatorium + World Radiation Center (PMO/WRC) Davos Dorf, Switzerland, July 1985.
- 4) Beardsley, R.C., Limeburner, H. Yu, and Cannon, G.A, Discharge of the Changjiang (Yangtze River) into the East China Sea, *Continental Shelf Research*, Vol.4, Nos. 1/2, 57-58, 1985.
- 5) http://daac.gsfc.nasa.gov/DAAC_DOCS/geomorphology/GEO_5/GEO_PLATE_D-5.HTML

THIS PAGE INTENTIONALLY LEFT BLANK

INITIAL DISTRIBUTION LIST

1. Defense Technical Information Center
Ft. Belvoir, VA
2. Dudley Knox Library
Naval Postgraduate School
Monterey, CA
3. CDR James A. Hill
Naval Postgraduate School
Monterey, CA 93943-5000
4. Chairperson, Department of Oceanography
Naval Postgraduate School
Monterey, CA 93943-5000
5. Chairperson, Department of Meteorology
Naval Postgraduate School
Monterey, CA 93943-5000
6. Professor Philip A. Durkee, MR/De
Naval Postgraduate School
Monterey, CA 93943-5000
7. Professor Steven R. Ramp, OC/De
Naval Postgraduate School
Monterey, CA 93943-5000